Applied Energy 317 (2022) 119148

Contents lists available at ScienceDirect

Applied Energy

journal homepage: www.elsevier.com/locate/apenergy

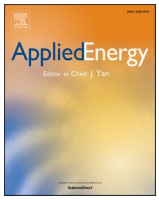

A dynamic performance diagnostic method applied to hydrogen powered aero engines operating under transient conditions

Yu-Zhi Chen [a], Elias Tsoutsanis [b,*], Heng-Chao Xiang [c], Yi-Guang Li [d], Jun-Jie Zhao [d]

[a] School of Power and Energy, Northwestern Polytechnical University, Xi'an, China
[b] Department of Mechanical Engineering, University of Birmingham, Edgbaston, Birmingham B15 2TT, UK
[c] China Gas Turbine Establishment, Aero Engine Corporation of China, Chengdu 610500, China
[d] School of Aerospace, Transport and Manufacturing, Cranfield University, Bedford, UK

HIGHLIGHTS

- The gas turbine model is validated by a well-used commercial software.
- An adapted sequential method is established for fault diagnosis of aero engines.
- Effect of heat soakage is considered in fault diagnosis under dynamic conditions.
- The economic impact of our method is assessed for hydrogen powered flights.
- The established method could diagnose faults successfully under dynamic states.

GRAPHICAL ABSTRACT

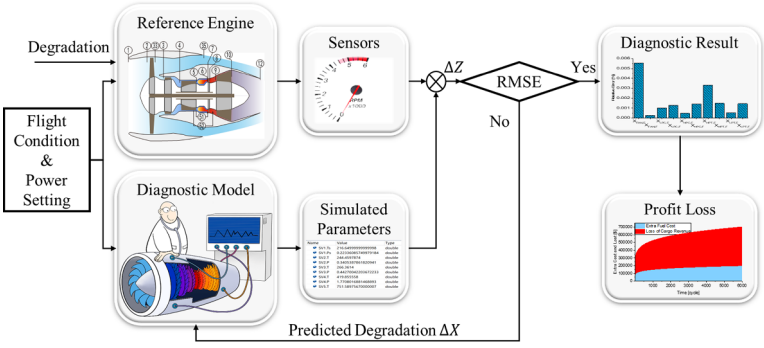

ARTICLE INFO

Keywords:
Aero Engine Performance
Condition Monitoring
Model-Based Method
Turbofan Engine Diagnostics
Economic Impact

ABSTRACT

At present, aero engine fault diagnosis is mainly based on the steady-state condition at the cruise phase, and the gas path parameters in the entire flight process are not effectively used. At the same time, high quality steady-state monitoring measurements are not always available and as a result the accuracy of diagnosis might be affected. There is a recognized need for real-time performance diagnosis of aero engines operating under transient conditions, which can improve their condition-based maintenance. Recent studies have demonstrated the capability of the sequential model-based diagnostic method to predict accurately and efficiently the degradation of industrial gas turbines under steady-state conditions. Nevertheless, incorporating real-time data for fault detection of aero engines that operate in dynamic conditions is a more challenging task. The primary objective of this study is to investigate the performance of the sequential diagnostic method when it is applied to aero engines that operate under transient conditions while there is a variation in the bypass ratio and the heat soakage effects are taken into consideration. This study provides a novel approach for quantifying component degradation, such as fouling and erosion, by using an adapted version of the sequential diagnostic method. The research presented here confirms that the proposed method could be applied to aero engine fault diagnosis under both steady-state and dynamic conditions in real-time. In addition, the economic impact of engine degradation on fuel cost and payload revenue is evaluated when the engine under investigation is using hydrogen. The proposed method

* Corresponding author.
E-mail address: e.tsoutsanis@bham.ac.uk (E. Tsoutsanis).

https://doi.org/10.1016/j.apenergy.2022.119148
Received 9 December 2021; Received in revised form 8 March 2022; Accepted 14 April 2022
Available online 26 April 2022

demonstrated promising diagnostic results where the maximum prediction errors for steady state and transient conditions are less than 0.006% and 0.016%, respectively. The comparison of the proposed method to a benchmark diagnostic method revealed a 15% improvement in accuracy which can have great benefit when considering that the cost attributed to degradation can reach up to $702,585 for 6000 flight cycles of a hydrogen powered aircraft fleet. This study provides an opportunity to improve our understanding of aero engine fault diagnosis in order to improve engine reliability, availability, and efficiency by online health monitoring.

Nomenclature

a	health index decay rate
A	Area $[m^2]$
AW	Auxiliary work $[W]$
b	exponential time-scaling parameter
BPR	Bypass ratio
C_{FG}	Nozzle coefficient
CM	Corrected mass flow
CN	Corrected engine shaft rotational speed
CP	Characteristic parameter
CW	Compressor work $[W]$
E	Residual error
EFC	Extra fuel cost [$]
EFF	Efficiency $[kg]$
EFW	Extra fuel weight
FAR	Fuel-air ratio
FC	Film coefficient $[(m^2 \bullet K)/W]$
H	Enthalpy $[kJ/kg]$
I	Shaft inertia $[kg \bullet m^2]$
k_m	Material thermal conductivity $[W/(m \bullet K)]$
l_{eff}	Effective length heat flow transport $[m]$
LCR	Loss of cargo revenue [$]
MN	Mach number
N	Shaft rotational speed $[rpm]$
NG	Net thrust $[N]$
NT	Net thrust $[N]$
Num_A	Number of aircrafts with the same type in airline fleet
Num_E	Number of engines per aircraft
OT	Operating time $[Second]$
P	Pressure $[atm]$
PR	Pressure ratio
Q	Heat rate $[W]$
R	gas constant [J/(kg • K)]
S	Entropy $[kJ/(kg \bullet K)]$
SP	Engine shaft surplus power $[W]$
T	Temperature $[Kelvin]$
TW	Turbine work $[W]$
U	Heat transfer coefficient $[W/(m^2 \bullet K)]$
UP	Unit price $[\$/kg]$
V	Velocity $[m/s]$
W	Mass flow rate $[kg/s]$
WAR	Water-air ratio
X	Degradation factor
Z	Gas path measurement

Greek Symbols

γ	Ratio of specific heats
ρ	Density $[kg/m^3]$
τ	Time constant $[s]$

Subscripts

amb	Ambient
BP	Fan bypass
$Core$	Fan core
$crit$	Critical condition
DP	Design point
g	Gas flow
ht	heat transfer
in	Inlet
m	Metal
OD	Off-design
out	Outlet
sn	Sonic condition
SLS	Sea-level standard

1. Introduction

As one of the engines of socio-economic growth, energy plays a paramount role in the evolution of modern society [1]. In recent years, an emerging body of research attention has been paid to energy consumption, for example, innovation cooperation and knowledge transfer that benefits energy technology progress and energy efficiency enhancement, which contributes to changes in energy consumption and low-carbon transition of energy structure [2]. Energy consumption market has long been dominated by fossil fuels, such as oil, coal and natural gas, which are the main sources of CO_2 and typical non-CO_2 greenhouse gases [3]. Attaining the global warming-limit goals, like 1.5 °C higher than the pre-industrial levels [4], should be largely equivalent to controlling conventional energy consumption. In addition, the non-fossil energy technologies [5] and low-carbon transition [6] are of great importance in the long term [7]. Recent years have seen renewed interest in hydrogen powered aero engines as it is clean, flexible, energy-efficient and can be produced from renewable sources. Some studies on hydrogen-based technologies could be referred to [8,9].

As reported by the International Civil Aviation Organization (ICAO), the passenger traffic and freight traffic are projected to rise annually from 2018 to 2038 by 4.2% and 3.5%, respectively [10]. Gas turbine engines play a critical role in civil aviation, particularly turbofan engines with a high bypass ratio which have the advantage of improved fuel consumption and propulsive efficiency [11]. It is reported that Rolls-Royce has a revenue of 11 billion USD per year from aero engine service and part replacement [12] indicating the importance of this area. Gas path measurements are associated with engine health and could be used for performance diagnosis to support condition based maintenance and reduce the cost of engine service [13,14]. It is noted that the performance diagnosis of gas turbines is crucially important to engine safety and efficiency for aircraft assets [15]. Consequently, the condition monitoring of gas turbines is a useful tool to improve their safety, reliability, and availability [16,17]. Currently, gas path analysis (GPA) is still one of the most effective ways for performance-based fault diagnosis of gas turbines [14]. The maintenance schedule conducted by the gas turbine performance specialist could be optimized by using the diagnostic results through GPA [18]. Typical gas path deterioration of gas turbines include fouling, erosion, corrosion, object damage, tip

Table 1
Overview of previous studies on gas turbine fault diagnosis when dealing with "smearing effect".

Research	Operating conditions	Research Object	Remarks
Jasmani et al. (2011) [30]	Steady-state	Industrial gas turbine	Sensor selection technique by using the measurement subset concept
Chen et al. (2015) [31]	Steady-state	Aero engine	Sensor selection platform to incorporate the health parameter correlation analysis
Xu et al. (2015) [32]	Steady-state	Aero engine	Optimal sensor selection method by considering sensor cost and fault detection rate
Simon and Rinehart (2016) [15]	Steady-state	Aero engine	Measurement choosing based on Kalman filter and a maximum a-posteriori
Hu et al. (2019) [33]	Steady-state	Chiller plant	Sensor selection method based on machine learning
Hu et al. (2021) [34]	Steady-state	Aero engine	Sensor selection by combining the nonlinear and linear engine models
Ogaji et al. (2002) [35]	Steady-state	Aero engine	Fault diagnosis based on multi-objective genetic algorithm
Stamatis (2011) [36]	Steady-state	Industrial gas turbine	Multiple steady-state operating points should be combined with parameter selection
Li and Ying (2018) [37]	Steady-state	Industrial gas turbine	Multiple operating points analysis to overcome the lack of measurement parameters
Chen et al. (2021) [29]	Steady-state	Industrial gas turbine	Sequential model-based diagnostic method
Tsoutsanis et al. (2015) [40]	Dynamic	Industrial gas turbine	Nonlinear adaptation of component maps
Tsoutsanis et al. (2016) [41]	Dynamic	Industrial gas turbine	Sliding window component map optimization for transient diagnostics and prognostics
Tsoutsanis et al. (2017) [42]	Dynamic	Industrial gas turbine	Real time diagnosis method incorporated in prognostics by examining the acceleration of degradation
Li and Ying (2020) [25]	Dynamic	Industrial gas turbine	Fault diagnosis scheme based on a steady-state model with dynamic measurements
Tsoutsanis et al. (2020) [19]	Dynamic	Industrial gas turbine	Real-time diagnosis method by dynamic tuners

clearance damage and thermal distortion [16].

Diagnostic methods are divided into three main sub-groups: model-based methods, data-driven methods, and hybrid methods [19]. The model-based methods [20] are one of the most well-known tools for assessing component degradation. However, they require expert knowledge for the development of engine performance models. With the advancement of computer technology, data-driven methods [21-24] have started to play an important role in fault diagnosis in recent years. However, the diagnostic performance relies heavily on available data and quality of training [25]. The hybrid methods [13] combine features from both model-based and data-driven methods to perform good diagnostic results [26]. It follows that there are various trade-offs between prediction accuracy and algorithm complexity [26]. There is no single method that can handle all the engine diagnostic challenges without any compromise. This study will focus on model-based methods, and those who are interested in data-driven and hybrid methods are prompted to [16,27,28] for more details.

The phenomenon of "smearing effect" causes more challenges to diagnostic systems to correctly identify the true degraded components [28]. The smearing effect occurs due to insufficient and inaccurate gas path measurements [29]. Typically, there are two ways to resolve this issue. The first one is to install more sensors in the engine gas path in order to provide redundant gas path information, which can help to reduce ambiguity and filter incorrect solutions. Jasmani et al. (2011) [30] proposed a sensor selection technique by using the measurement subset concept for improving the precision of fault diagnostics. Chen et al. (2015) [31] implemented a sensor selection platform to incorporate the health parameter correlation analysis for fault diagnosis. Xu et al. (2015) [32] used an optimal sensor selection method by considering sensor cost and fault detection rate through multiple objective optimizations. Simon and Rinehart (2016) [15] suggested that the measurement choosing method could be applied to performance modelling and fault quantification by a Kalman filter and a maximum a-posteriori. Hu et al. (2019) [33] designed a sensor selection method based on machine learning which incorporated the actual and virtual sensor for fault detection. Hu et al. (2021) [34] suggested an optimization scheme for sensor selection by combining the nonlinear and linear engine models to increase the computation speed. However, the increasing number of sensors will cause sensor-related problems such as increasing the configuration complexity and operating costs [32], extra flow disturbances [29], and additional weight. Moreover, the appended sensors could be a good option for industrial engines, but it is not an attractive solution for aero engines that are in pursuit of high power to weight ratio.

A second way to address insufficient gas path measurements is to use the measurements at multiple operation points. It follows that we can use multiple steady-state operating points and/or operating points under transient conditions. Several studies in the area of fault diagnosis utilize gas path measurements extracted from multiple operating points under steady-state conditions. Ogaji et al. (2002) [35] introduced an engine diagnostic method by multi-objective genetic algorithm, and each objective refers to the diagnostic error of every single operating point. Stamatis (2011) [36] suggested the multiple steady-state operating points should be combined with parameter selection to assure the effectiveness of diagnosis. Li and Ying (2018) [37] applied the multiple operating points analysis to overcome the lack of measurement parameters for gas turbine fault quantification. Chen et al. (2021) [29] presented a sequential model-based diagnostic method based on multiple operating points under steady-state conditions. However, gas path measurements from multiple steady-state operating points are not always available in practice [38,39]. Consequently, gas path analysis based on multiple steady-state operating points may not provide a high-quality insight into the engine condition when the majority of its operation might be under transient conditions or quasi-transient conditions. Therefore, another family of research works have focused on utilizing transient data for diagnostic purposes. Tsoutsanis et al. (2015) [40] performed diagnostics of engine faults by nonlinear adaption of component maps using transient gas path measurements with the accuracy of fault diagnostic close to 99%. In 2016 and 2017, the dynamic fault diagnosis scheme is adapted and integrated with the regression method for fault prognosis based on local window-based segments [41,42]. Li and Ying (2020) [25] introduced a fault diagnosis scheme based on a steady-state model with dynamic measurements. Tsoutsanis et al. (2020) [19] introduced a real-time diagnosis method with multiple component faults simultaneously. The above studies highlighted that it is another effective alternative to incorporate gas path measurements at dynamic conditions in gas turbine diagnostics. However, the basic principle of fault diagnosis by multiple points at steady-state and transient conditions is the same in the sense that the main reason for using multiple operation points is to improve the accuracy of diagnosis. It is worth emphasizing that the smearing effect could not always be avoided by multiple operation points analysis [29]. Moreover, the aforementioned fault diagnostic methods have not taken into account the heat soakage effects during dynamic operation. Li et al. (2020) [43] highlighted that the heat soakage effect would delay the net thrust of a turbojet engine by 2.5% at the end of manoeuvre. Hence, it is more realistic to consider the heat soakage effect for fault diagnosis under transient conditions.

It is evident from the brief literature review above that there has been a ubiquitous recognition of the problems associated with the "smearing effect" in fault diagnosis. A summary of previous research

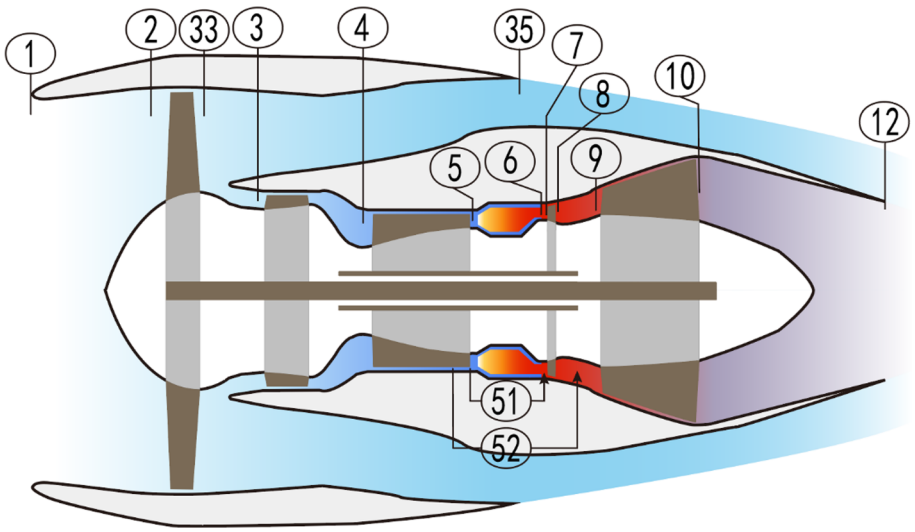

Fig. 1. Configuration of turbofan engine in concern and its station numbering.

Table 2
Turbofan engine measurements on-wing [45].

No	Measurement	Symbol
1	Ambient pressure	P_1
2	Ambient temperature	T_1
3	Bypass inlet pressure	P_{33}
4	Low-pressure compressor (*LPC*) exit pressure	P_4
5	*LPC* exit temperature	T_4
6	High-pressure compressor (*HPC*) exit pressure	P_5
7	*HPC* exit temperature	T_5
8	Low-pressure turbine (*LPT*) inlet pressure	P_9
9	*LPT* inlet temperature	T_9
10	*LPT* exit pressure	P_{10}
11	*LPT* exit temperature	T_{10}
12	Flight Mach Number	*MN*
13	*LP* shaft rotational speed	N_{LP}
14	*HP* shaft rotational speed	N_{HP}
15	Burner fuel flow rate	W_{Fuel}

works is presented in Table 1. It is clear that the majority of the research studies has focused on steady-state conditions, with only a few studies dealing with dynamic operating conditions.

To summarize, this study explores a more sophisticated and realistic approach by improving the sequential model-based method and applying it for a turbofan engine in order to demonstrate its advantages in handling fault diagnosis of the engine under transient conditions. In contrast to our earlier work [29], where the shaft power compatibility between turbine and compressor is necessary for the sequential method, this study proposes an advanced diagnostic method that is suitable for both steady-state and dynamic conditions. Moreover, our previously published study [29] is limited to single-pass flow engines such as industrial gas turbines, turbojets and turboprops. In this study, the sequential method is adapted to deal with double flow turbofan engines by assigning the bypass ratio according to the exhaust flow and fan inlet flow. Both steady-state and transient engine models are developed and validated with commercial software. In addition, the heat soakage is integrated with the developed engine performance model to make engine dynamic conditions more realistic. This study aims to contribute to this growing area of research by exploring gas path analysis under transient conditions for a turbofan engine and the main contributions are listed as follows:

1) The adapted method could extend the sequential model-based approach for the turbofan engine as the bypass ratio varies with operating conditions.
2) Aside from the gas path analysis under steady-state conditions, the performance diagnosis under transient conditions is investigated, which could overcome the lack of steady-state operation points during flight trajectory. While our previous work [29] was applied for steady state conditions, this study addresses the applicability of the method for transient operating conditions.
3) So far, existing fault diagnosis studies under transient conditions utilize multiple measurement sets during the dynamic trajectory. However, it has been shown that fault diagnosis using multiple points could not guarantee the mitigation of the smearing effect at all times. Hence, the sequential method is incorporated in this study, for the first time, to address the smearing effect by using dynamic measurements. This approach can resolve the issue of the lack of multiple steady-state operation points for aero engines.
4) The increasing number of degraded components will increase the complexity and nonlinear performance diagnosis [28]. The proposed scheme of performance diagnostics can cope with simultaneous degradation of all five rotating components under steady-state and transient conditions and can also be used for real-time performance evaluation.
5) The effect of engine degradation on the economic aspect is assessed through typical flight missions that are characterized by time evolving fault propagation.

The remaining part of the paper is organized as follows. Section 2 presents the methodology of the proposed approach. Section 3 of this paper examines and validates the developed gas turbine performance model. Section 4 presents the results and discussions of this research study according to the examined case studies before we draw some conclusions at the end of the paper.

2. Methodology

2.1. Assumptions

The following assumptions were made to focus on testing the proposed method's effectiveness and capabilities in this study.

- Measurement noise/bias is excluded in this study as the main focus is on enriching the fault diagnosis method rather than the sensor-related problems.
- Simultaneous time-evolving soft degradation of all components is considered. Moreover, degradation development pattern follows an exponential tendency of health indexes with respect to time.

Table 3
Degradation factors regarding turbofan engine in concern.

Component	Symbol		Health Parameter
FAN	X_{FAN}	$X_{FAN,E}$	Degradation factor of *FAN* efficiency
		$X_{FAN,F}$	Degradation factor of *FAN* flow capacity
LPC	X_{LPC}	$X_{LPC,E}$	Degradation factor of *LPC* efficiency
		$X_{LPC,F}$	Degradation factor of *LPC* flow capacity
HPC	X_{HPC}	$X_{HPC,E}$	Degradation factor of *HPC* efficiency
		$X_{HPC,F}$	Degradation factor of *HPC* flow capacity
HPT	X_{HPT}	$X_{HPT,E}$	Degradation factor of *HPT* efficiency
		$X_{HPT,F}$	Degradation factor of *HPT* flow capacity
LPT	X_{LPT}	$X_{LPT,E}$	Degradation factor of *LPT* efficiency
		$X_{LPT,F}$	Degradation factor of *LPT* flow capacity

Table 4
Fault propagation related coefficients [48].

Component	Health Parameter	Degradation Range [48]	Coefficient	Value
FAN	$X_{FAN,E}$	0 ~ -2.85 %	*a*	0.01
			b	0.11878
	$X_{FAN,F}$	0 ~ -3.65 %	*a*	0.01
			b	0.14675
LPC	$X_{LPC,E}$	0 ~ -2.61 %	*a*	0.01
			b	0.1088
	$X_{LPC,F}$	0 ~ -4.00 %	*a*	0.01
			b	0.1571
HPC	$X_{HPC,E}$	0 ~ -9.40 %	*a*	0.01
			b	0.25236
	$X_{HPC,F}$	0 ~ -14.06 %	*a*	0.01
			b	0.29621
HPT	$X_{HPT,E}$	0 ~ -3.81 %	*a*	0.01
			b	0.1516
	$X_{HPT,F}$	0 ~ +2.57 %	*a*	0.01
			b	0.10705
LPT	$X_{LPT,E}$	0 ~ -1.078 %	*a*	0.01
			b	0.008
	$X_{LPT,F}$	0 ~ +0.4226 %	*a*	0.001
			b	0.16544

- The efficiency and mass flow capacity factors are used to represent component degradation. Additionally, the pressure ratio factor is assumed to have the same magnitude as the flow capacity factor, when considering compressor fouling and turbine erosion [44].
- All the turbofan engines on-wing have the same fault development pattern for techno-economic evaluation purposes.

2.2. Engine models

A dual-shaft turbofan engine, similar to CFM56-7B installed on Boeing 737–800 aircraft as shown in Fig. 1 is used in this study. It includes a fan, two compressors, a combustor, and two turbines with separated exhaust nozzles. Table 2 [45] summarizes the CFM56-7B engine measurements on-wing in Boeing 737–800 fleet. The turbofan engine performance model is one of the key elements for model-based performance diagnostics [46]. A thermodynamic model for turbofan engine in concern has been developed in this study for both steady-state and transient conditions. The transient performance simulation model is based on constant mass flow method [43] with the consideration of heat soakage. The more details of performance simulation for the aero engine performance under steady-state and dynamic conditions are summarized in Appendix A. The fuel flow is selected as the control input parameter, although other parameters such as shaft rotational speed, and turbine inlet temperature could be selected.

2.3. Degradation modelling

2.3.1. Degradation factor

Generally, the turbofan engine's actual performance depends on the performance of each component [42]. Hence, the degradation factor (X) is determined by Eq. (1) to represent the health state of each characteristic parameter for different components [47]. When X equals to one, the real characteristic parameter has the same value as the characteristic parameter under a healthy state. Table 3 lists the degradation factors relevant to the aero engine examined in this study.

$$X = \frac{CP_r}{CP_h} \tag{1}$$

where the subscript "r" and "h" represent the component characteristic under real/actual and clean/healthy conditions, respectively.

2.3.2. Degradation propagation modelling

The typical degradation level of turbofan engines at 6000 cycles is demonstrated in Table 4 [48] while all five rotating components are suffering from performance deterioration simultaneously. Hence, the

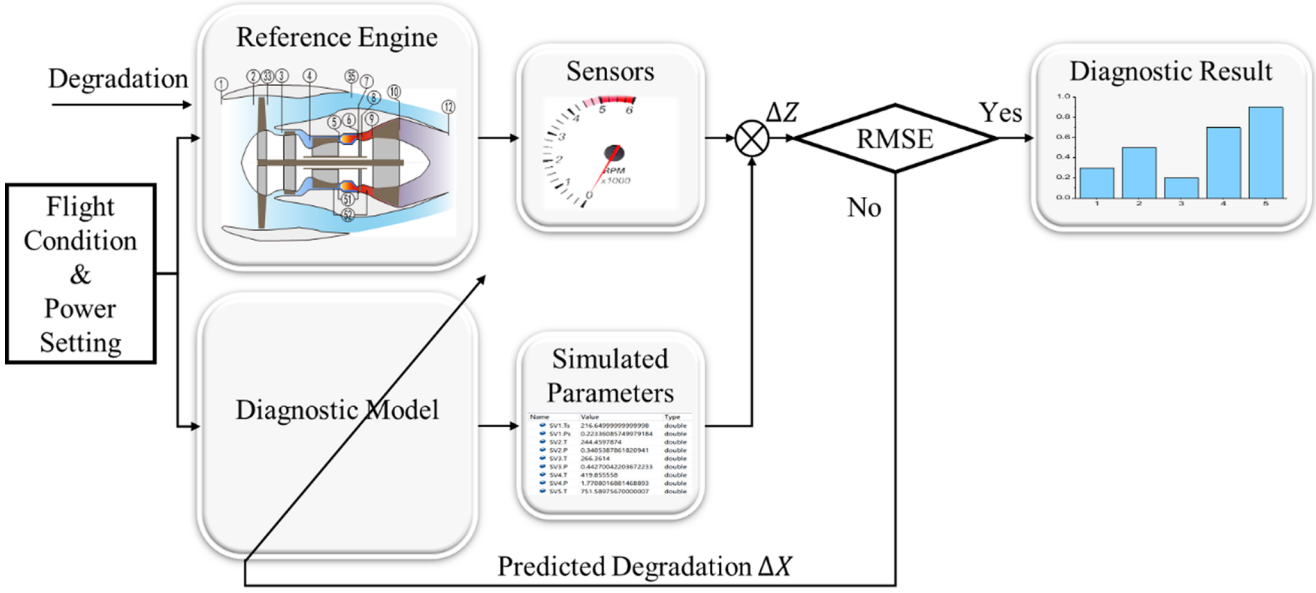

Fig. 2. Flow chart of diagnostic tuner process.

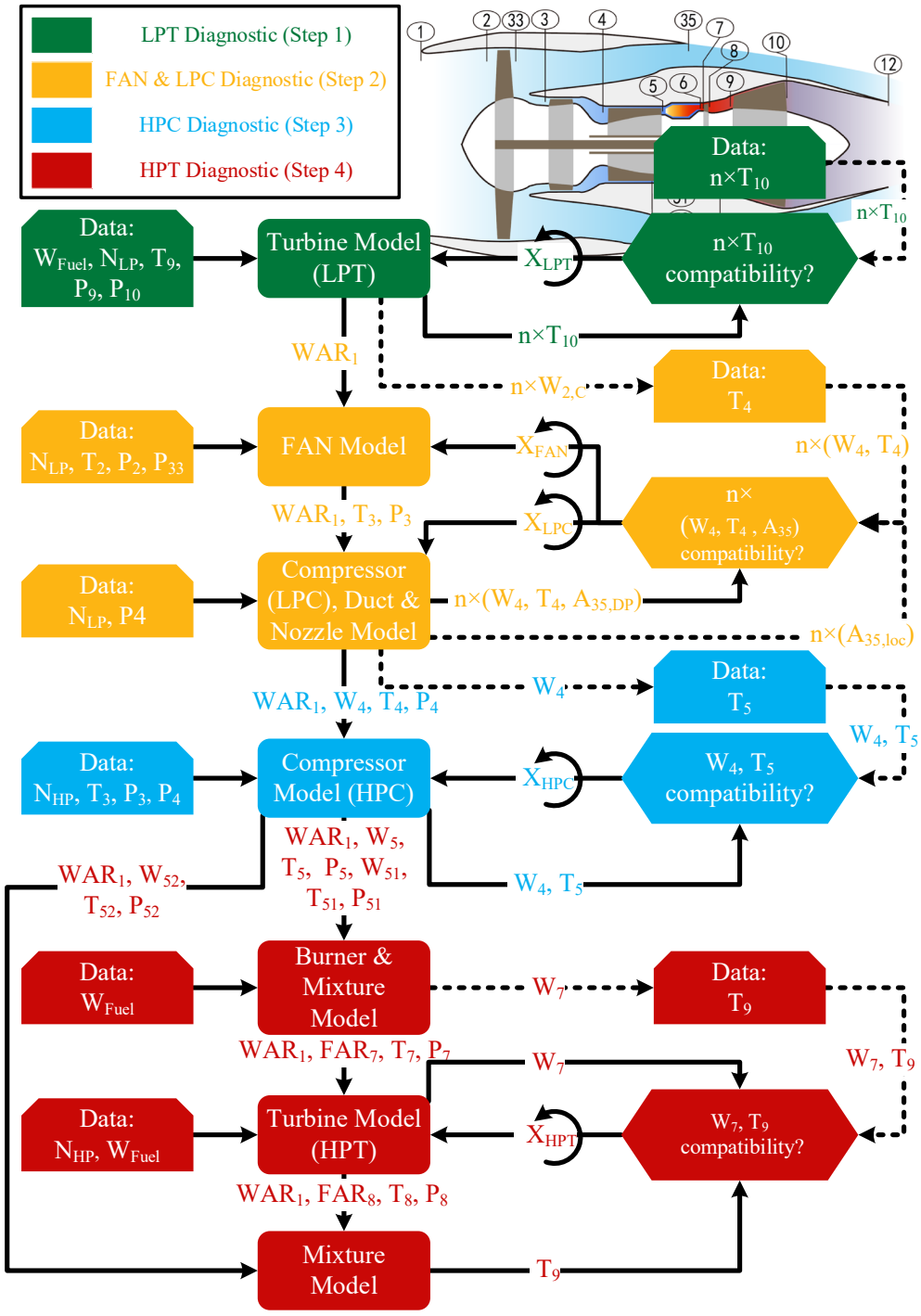

Fig. 3. Sequential diagnostic scheme of gas turbine.

number of cycles at failure is defined as 6000 cycles for the aero engine concerned in this study. In general, the exponential rate of change is one of the most widely used groups of degradation propagation models [49]. Moreover, the hypothesis of fault propagation and actual observation trends are consistent [47] and chosen in this study.

The degradation propagation model could be defined by Eq. (2) [49], which assumes the exponential curve relationship between flight cycles and deterioration evolution.

$$|\Delta X| \bullet X = |CP_r - CP_h| = 1 - exp(a \bullet t^b) \tag{2}$$

where a is the decay rate of health index, b is the exponential time-scaling coefficient, and t is the flight cycle.

The coefficients a and b are derived in Table 4 to represent the fault propagation with the flight cycle. It is worth noting that ΔX in Eq. (2) is positive for turbine flow capacity representing erosion, where the rest is negative. Table 4 also presents the range of degradation factors for each rotating component regarding the efficiency and flow capacity.

2.4. Techno-economic evaluation of gas path fault

During the fault propagation, the fuel consumption will be increased to maintain the same thrust during each flight segment. Moreover, if constant take-off weight is assumed, the cargo weight needs to be decreased, corresponding to the additional fuel weight in aircraft. The

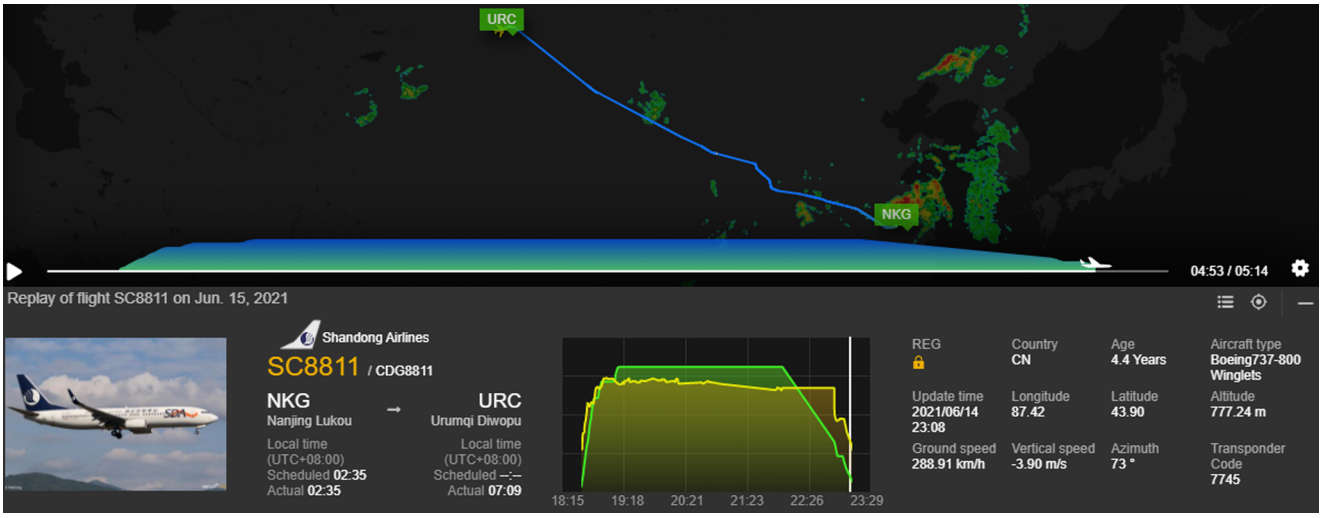

Fig. 4. Replay of flight SC8811 executed by a Boeing 737–800 powered by two CFM56-7B engines [50].

Table 5
Engine specification.

Parameter	Symbol	Unit	Value
Flight Mach Number	*MN*	–	0.8
Altitude	*ALT*	m	11,000
Delta Pressure from ISA	ΔP_1	atm	0.0
Delta Temperature from ISA	ΔT_1	Kelvin	0.0
Ambient Relative Humidity	RH_1	%	0.0
Inlet Airflow Rate	W_1	kg/s	221.865
LP Rotational Speed	N_{LP}	rpm	4000
HP Rotational Speed	N_{HP}	rpm	18,000
Fuel Flow rate	W_{Fuel}	kg/s	0.1876
Fuel Heating Value	*FHV*	MJ/kg	118.429
Core Fan Pressure Ratio	PR_{Core}	–	1.3000
Bypass Fan Pressure Ratio	PR_{BP}	–	1.7017
Bypass Ratio	*BPR*	–	9.0000
LPC Pressure Ratio	PR_{LPC}	–	4.0000
HPC Pressure Ratio	PR_{HPC}	–	6.5000
Power Offtake	*PWX*	kW	50.0

Table 6
Design point model validation [51].

Symbol	Units	GasTurb [51]	ThermoWorks	Prediction Error [%]
T_1	Kelvin	216.65	216.65	0.000
P_1	atm	0.2234	0.2234	0.000
T_2	Kelvin	244.44	244.46	0.008
P_2	atm	0.3406	0.3405	0.029
T_3	Kelvin	266.35	266.36	0.004
P_3	atm	0.4428	0.4427	0.023
T_4	Kelvin	419.80	419.86	0.014
P_4	atm	1.7710	1.7708	0.011
T_5	Kelvin	751.64	751.59	0.007
P_5	atm	11.5116	11.5102	0.012
T_6	Kelvin	1600.00	1597.30	0.169
P_6	atm	10.9360	10.9347	0.012
T_7	Kelvin	1561.00	1559.01	0.127
P_7	atm	10.9360	10.9347	0.012
T_8	Kelvin	1280.00	1281.69	0.132
P_8	atm	4.0559	4.0617	0.143
T_9	Kelvin	1252.03	1253.72	0.135
P_9	atm	4.0559	4.0617	0.143
T_{12}	Kelvin	776.95	779.84	0.372
P_{12}	atm	0.4346	0.4368	0.506
T_{33}	Kelvin	290.18	290.19	0.003
P_{33}	atm	0.5796	0.5795	0.017
T_{35}	Kelvin	290.18	290.19	0.003
P_{35}	atm	0.5651	0.5650	0.018

extra fuel weight (*EFW*) consumed for each engine could be computed by the fuel flow rate (W_{Fuel}) during each flight segment multiplied by the corresponding operating time as follows:

$$EFW = \sum_i^n \left[\left(W_{Fuel,i,r,} - W_{Feul,i,h,} \right) \times OT_i \right] \tag{3}$$

where *OT* is operating time, *i* is i-*th* flight segment, *n* is the number of flight segments to be considered, and the subscripts of "*r*" and "*h*" are described in Eq. (1).

As the *EFW* is known, the extra fuel cost (*EFC*) for the entire airline fleet could be calculated by Eq. (4).

$$EFC = EFW \times UP_{Fuel} \times Num_E \times Num_A \tag{4}$$

where UP_{Fuel} is the unit price of fuel, Num_E represents the number of engines per aircraft, Num_A denotes the number of aircrafts of the same type in the airline fleet.

Similarly, the loss of cargo revenue (*LCR*) for the airline fleet could be obtained by (5) which represents payload compensation.

$$LCR = EFW \times UP_{Cargo} \times Num_E \times Num_A \tag{5}$$

where UP_C is the unit revenue of flight payload.

2.5. Sequential diagnostic under steady-state condition

The non-liner gas path analysis [19] could be represented by Eq. (6) where *Z* denotes gas path measurements and $f(\bullet)$ is the system function of the model in concern. In traditional gas path analysis method, $f(\bullet)$ represents the gas turbine engine model. In the proposed sequential method, $f(\bullet)$ denotes the sub-models in concern in each sequential step. In the diagnosis process, *X* is iteratively evaluated by the Newton-Rapson method in order to match the targeted measurement (*Z*).

$$Z = f(X) \tag{6}$$

The research flow chart is presented in Fig. 2 where the health parameters are iterated to satisfy the reference engine measurements. The structure of the sequential diagnostic method for the turbofan engine can be divided into four sequential steps, as shown in Fig. 3. The dotted lines indicate the information flow of target parameters obtained by actual gas path measurements or virtual measurements from the previous diagnostic steps. The first step in this process is to quantify the degradation of *LPT* and identify the core inlet mass flow rate of the engine. The second step will identify the degradation level involved in *FAN* and *LPC*. In the follow-up phase, fault detection of *HPC* will be conducted before conducting the *HPT* diagnostics. Rounded rectangles

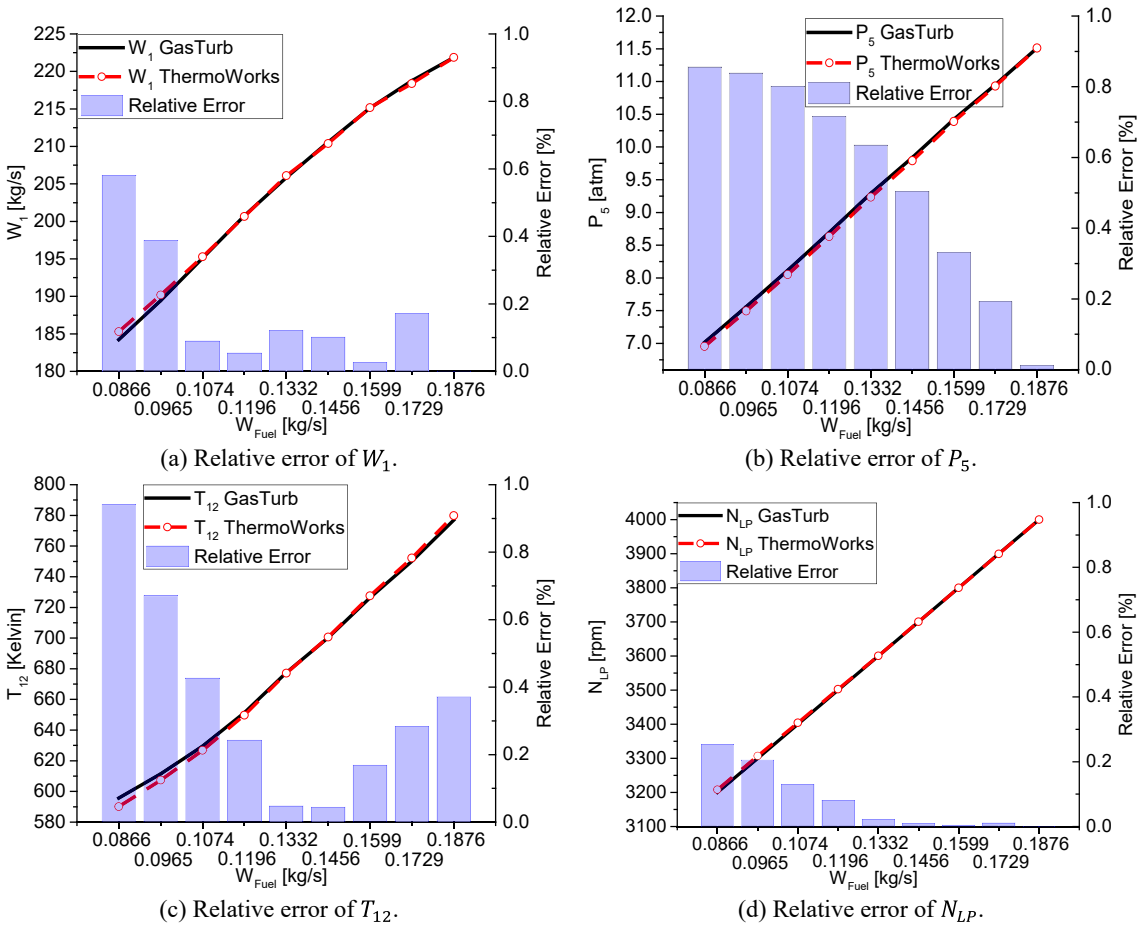

(a) Relative error of W_1. (b) Relative error of P_5.

(c) Relative error of T_{12}. (d) Relative error of N_{LP}.

Fig. 5. Off-design model validation [51].

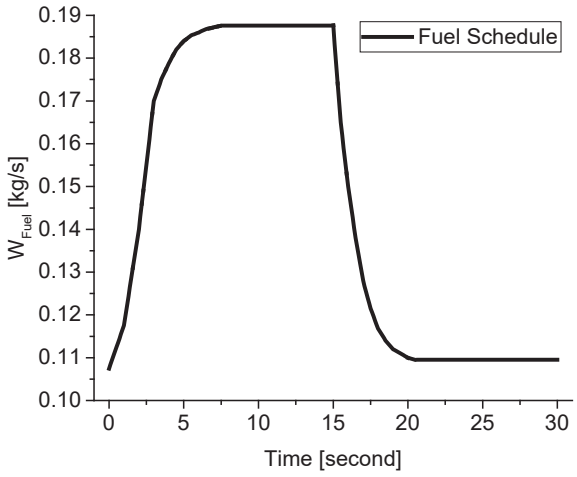

Fig. 6. Acceleration fuel schedule with CN_{FAN} from 75% to 100%.

represent the models required in each step, and snip same slide corner rectangle (most of them are in the first column) represents the available measurements on-wing. The arc with arrows illustrates the iterations, and the final hexagons trace the error between the to-be-adapted value and targeted value. The diagnostic scheme is shown in the following steps:

- Step 1: Low-Pressure Turbine Fault Quantification

The first step in this scheme is to quantify the X_{LPT} ($X_{LPT,E}$, $X_{LPT,F}$) by adjusting the *LPT* component map through an iterative process to fulfil the matching of exhaust gas temperature (T_{10}).

- Step 2: Fan and Low-Pressure Compressor Fault Quantification

Once the *LPT* diagnostic has been completed, the second step is to evaluate X_{FAN} ($X_{FAN,E}$, $X_{FAN,F}$) and X_{LPC} ($X_{LPC,E}$, $X_{LPC,F}$) by scaling the *FAN* and *LPC* maps according to *LPC* outlet mass flow rate (W_4), *LPC* outlet temperature (T_4), and required nozzle outlet area (A_{35}).

- Step 3: High-Pressure Compressor Fault Quantification

Then, X_{HPC} ($X_{HPC,E}$, $X_{HPC,F}$) are adjusted to scale the *HPC* component map on the basis of *HPC* inlet mass flow rate (W_4) and *HPC* outlet temperature (T_5).

- Step 4: High-Pressure Turbine Fault Quantification

Finally, X_{HPT} ($X_{HPT,E}$, $X_{HPT,F}$) are tuned to scale the *HPT* component map based on *HPT* inlet mass flow rate (W_7) and *LPT* inlet temperature (T_9).

The bypass ratio in Step 2 is decided by Eq. (A.7) in Appendix A, where the core mass flow is obtained from Step 1, and the fan inlet mass flow is calculated in the fan model by Eq. (A.2) in Appendix A. In addition, the required bypass nozzle area is employed as one of the convergence criteria to address unknown bypass mass flow rate in Step 2.

The term 'n' is used in this paper to refer to the number of operating points. It is necessary here to clarify that the first two steps need three

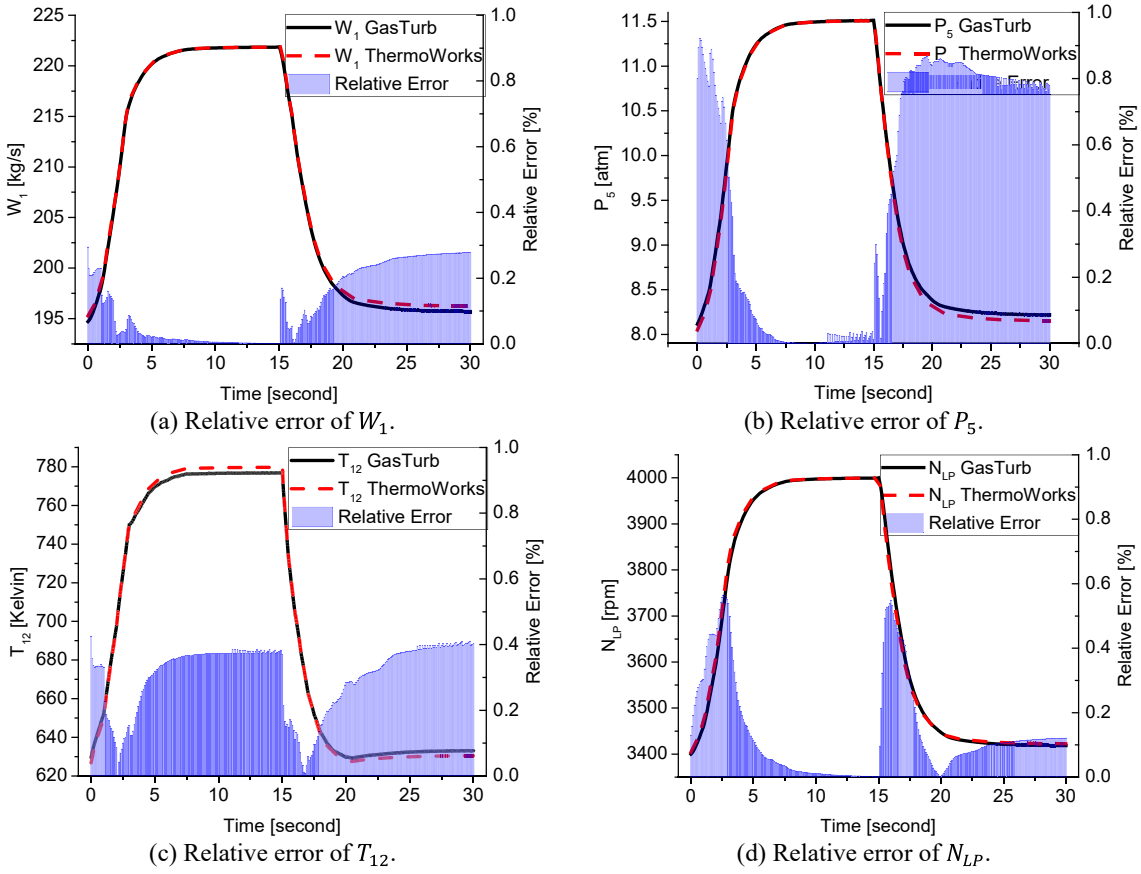

(a) Relative error of W_1. (b) Relative error of P_5.

(c) Relative error of T_{12}. (d) Relative error of N_{LP}.

Fig. 7. Engine model validation at transient manoeuvre [51].

operation points, and the final two steps need only one operating point. It is a significant advantage of the sequential method that can tailor the operating point for different engine components to reduce the computation time.

2.6. Sequential diagnostics under transient conditions

As demonstrated in our earlier works [29], the sequential diagnostic could achieve high precision and fast computation even when all components are concurrently degraded at steady-state conditions, for single-pass flow engines. However, the method requires multiple (three) operating points to diagnose the health condition of some components with limited gas path measurements. Moreover, the fault diagnosis scheme showed in Steps 1 and 2 of Section 2.5 also requires multiple operation points. Nevertheless, it may not be feasible to obtain enough operating points under steady-state conditions for a commercial engine during each flight cycle. In practice, the steady-state operating condition could frequently be available during the cruise phase of the flight envelope.

Fig. 4 [50] demonstrates a typical flight trajectory of a commercial aircraft where the yellow, green and blue lines represent the ground speed, altitude and flight path, respectively. It is clear, from Fig. 4, that the altitude is changing all the time except at the cruising state, and steady-state conditions are mainly present at cruise conditions. Although several different ground speeds exist during the cruise condition in Fig. 4, the engine operating states are very close to each other as the velocities present only small variations and are not suitable for fault diagnosis based on multiple operating points. In such conditions, a sequential diagnostic under transient condition is proposed that uses both steady-state and transient measurements to quantify the fault level of each component. For *LPT*, *FAN* and *LPC* diagnosis, the proposed method will be fed by the engine measurements from an initial steady-state point to a specified time of a transient manoeuvre. For *HPC* and *HPT*, the diagnostic method will only need the initial steady-state operation measurements.

3. Engine model validation

Fig. 1 demonstrates the schematic of the dual-shaft turbofan engine, which is similar to the CFM56-7B engine. The developed gas turbine thermodynamic model has been validated using a well-known commercial software GasTurb [51], at both steady-state and transient conditions. The design point specifications of the aero engine in concern are shown in Table 5. There is a growing body of literature that recognizes the importance of energy structure for the target of carbon neutrality. Moreover, hydrogen fuel will play a critical role in the potential carbon reduction around global aviation. In addition, it is worth noting that the first commercial aircraft powered by hydrogen has been launched successfully in 2020 [52]. Hence, the hydrogen fuel is selected in this study.

3.1. Steady-state model validation

The steady-state model consists of two parts: design point algorithm and off-design algorithm. Table 6 presents the results obtained from the developed model (ThermoWorks) and GasTurb, where the maximum prediction error is under 0.51% for different engine stations in concern. It is evident from this table that the developed model achieved high precision at the design point.

The aero engine operates in different working conditions during the flight envelope. Hence, it is necessary to conduct the steady-state off-design performance validation for the ThermoWorks engine model. Both GasTurb and ThermoWorks use the same component maps for model

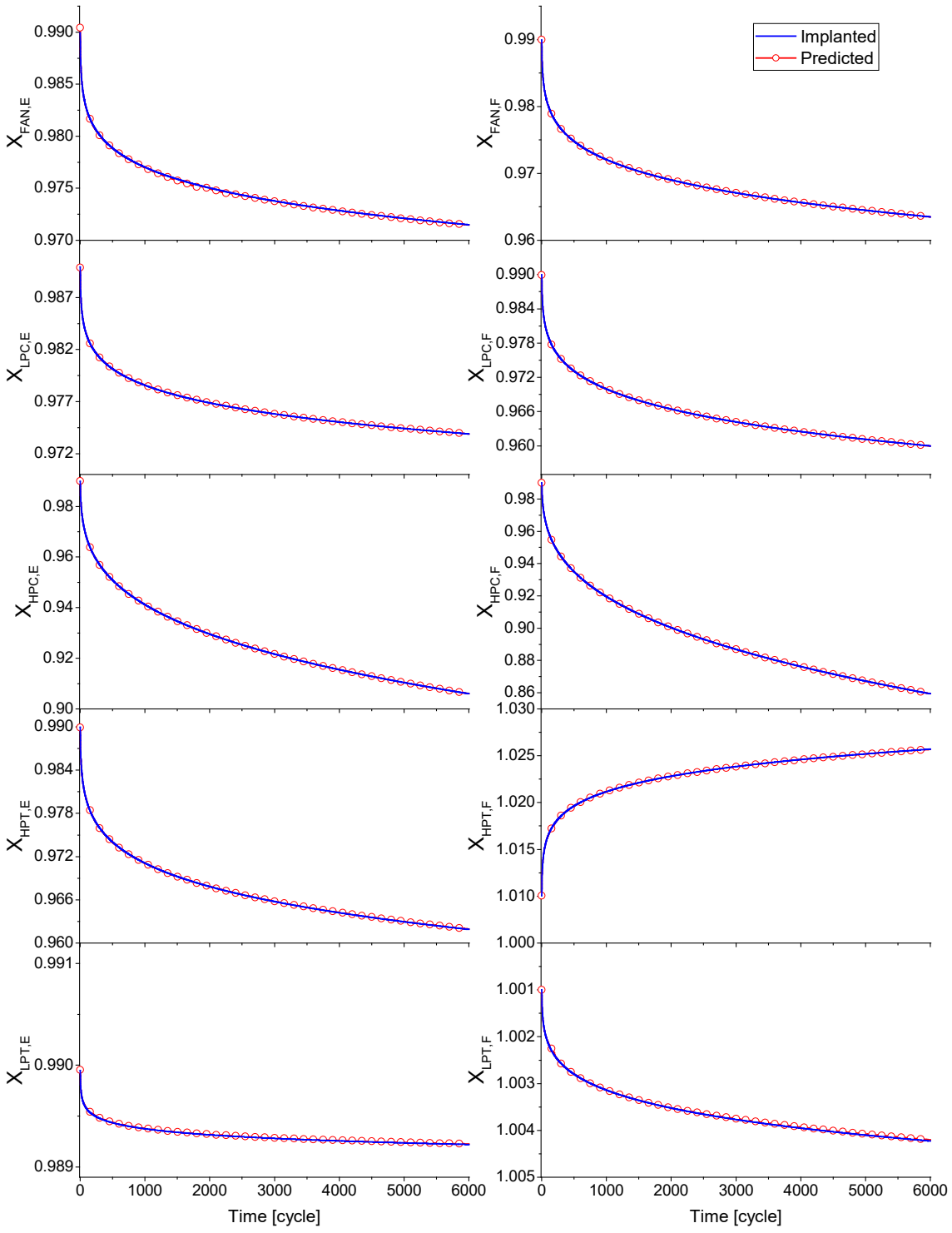

Fig. 8. Implanted and predicted damage propagation in Case 1.

validation. The fuel flow is the control input in ThermoWorks engine model to obtain the performance parameters and is obtained through GasTurb at different relative corrected fan rotational speed (CN_{FAN}), varying from 80% to 100% with a step of 2.5%. A comparison is made between the GasTurb and the ThermoWorks that is shown in Fig. 5, including four performance parameters. More specifically, engine inlet airflow rate (W_1), *HPC* outlet pressure (P_5), core nozzle outlet temperature (T_{12}), fan rotational speed (N_{LP}) are demonstrated with a variation of engine fuel flow rate.

A comparison between GasTurb and ThermoWorks reveals high prediction precision for different steady-state working conditions. For a low power setting, the maximum relative error is raised slightly within reasonable bounds. This deviation is justified by the fact that different component map reading methods are involved in GasTurb and the developed model. The highest prediction error among each parameter is 0.86% and is observed for P_5 at 80.0% relative corrected fan rotational speed as shown in Fig. 5(b). The developed performance model maintains a sustained high degree of precision, despite the error increase at low operating conditions. Hence, the sequential diagnostic will be implemented on the developed model for fault detection, isolation, and

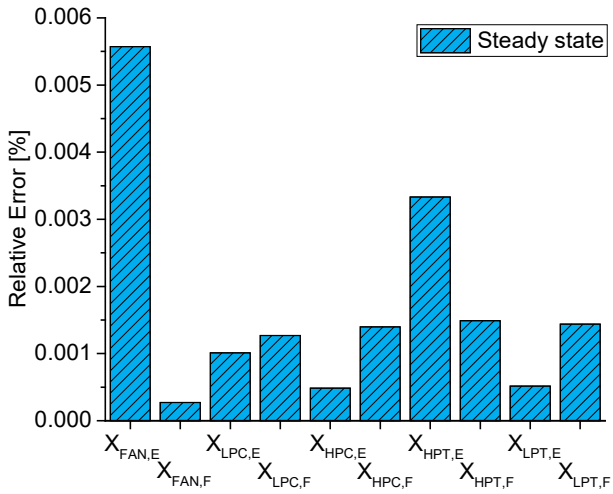

Fig. 9. Average prediction error of degradation factors in Case 1.

Table 7
Computational efficiency of the diagnostic model in Case 1.

Parameter	Symbol	Unit	Step 1	Step 2	Step 3	Step 4
Run Time	*RT*	Second	0.014	0.041	0.015	0.011
Operating Point	*n*	–	3	3	1	1

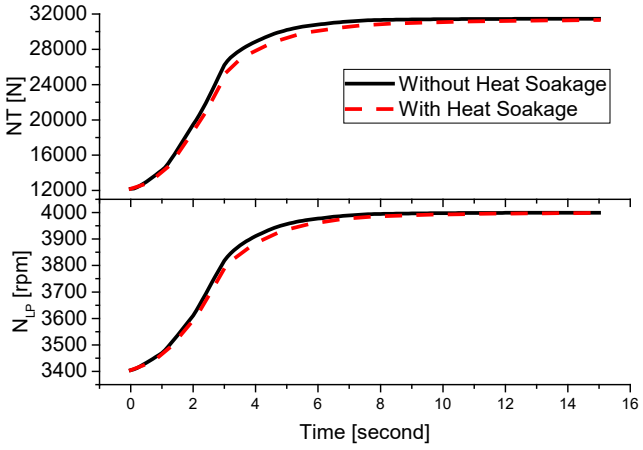

Fig. 10. Effect of heat soakage during transient manoeuvre.

identification.

3.2. Transient model validation

Model validation at transient conditions is another prerequisite for carrying out diagnostics based on transient engine data. A 15 s acceleration manoeuvre is conducted with CN_{FAN} increasing from 85% to 100% firstly. Then, a 15 s deceleration manoeuvre is initiated with CN_{FAN} decreasing from 100% to 85%. The fuel schedule is shown in Fig. 6 where a time step of 0.1 s is used in both GasTurb and the developed engine model.

The four performance parameters obtained from GasTurb and the developed model are presented in Fig. 7. What stands out from Fig. 7 is that there is a good agreement between the GasTurb and ThermoWorks. The highest prediction error is less than 0.92% for all the performance parameters, which is the P_5 at 0.2 s during the acceleration manoeuvre. Therefore, the developed model is sufficiently good as a baseline engine model for examining fault diagnosis at transient conditions.

4. Application and analysis

4.1. Case study description

Three case studies are carried out in the following subsection in order to demonstrate the improvements in computational efficiency and diagnostic accuracy that the proposed method has in comparison with a well-used benchmark method published in 2020 [25]. The objective of the three case studies are as follows:

Case 1. *The objective of this study is to assess the diagnostic capability of the proposed method when applied to a turbofan engine with its bypass ratio varying with operating conditions under state-state condition.*

Case 2. *This case study seeks to evaluate the computational performance and diagnostic prediction of the proposed method for fault diagnosis under dynamic conditions and compare it with a benchmark method [25] so as to demonstrate the advantages of the new method.*

Case 3. *The objective of this case study is to evaluate the economic impact of our proposed method by testing it under a time evolving engine component fault propagation for a series of flight cycles.*

4.2. Case 1: Sequential diagnostic under steady-state condition

The fault diagnosis is based on the scheme shown in Fig. 3 when the engine is experiencing simultaneous degradation in all five engine components. The *LPT* fault diagnosis is conducted first and followed by the combination of *FAN* and *LPC* diagnosis. In order to assess the proposed sequential method, repeated diagnosis during degradation propagation was conducted. Fig. 8 compares the diagnostic results of the ten health parameters among 6000 flight cycles. As it can be seen from the figure, it is apparent that the predicted degradation factors are extremely close to the actual implanted value, which shows the success of the diagnosis.

If we now turn to the quantitative analysis of the diagnostic results under the steady-state condition, the average relative error of each degradation factor among 6000 flight cycles is summarized in Fig. 9. It is evident that the highest prediction error is less than 0.006% for all ten health parameters during the degradation process. Further statistical tests reveal the computation efficiency of the proposed sequential method in Table 7. What stands out from the table is that the average computation time is 0.014, 0.041, 0.015, and 0.011 s for four sequential steps, respectively. The ten health parameters corresponding to five simultaneously degraded engine components are computed in 0.081 s. The diagnosis process is computed via Visual Studio software on a personal computer with Intel(R) Core (TM) i7-4910MQ CPU @2.90 GHz and 16 GB RAM. Moreover, the operating points needed for each step are also shown in Table 7. Only the first two steps need three operating points, while the last two steps only need one operating point which has also mentioned in the methodology section. This is one of the primary benefits of the proposed sequential diagnosis method.

In summary, these results show that the developed gas path analysis method could capture the degradation's propagation accurately and robustly in a computationally efficient manner, even when the degradation level changes with respect to flight cycles.

4.3. Case 2: Sequential diagnostic under dynamic condition

To distinguish transient performance with and without considering heat soakage, a comparison has been made during a 15 s acceleration with the same fuel schedule, as presented in Fig. 6. It is evident from Fig. 10 that the heat transfer between engine metal and gas flow will delay the transient response during the dynamic manoeuvre. Based on the given fuel schedule, the maximum delay of net thrust and *LP* shaft speed is 5.06% at 3.1 s and 0.85% at 3.3 s, respectively. However, the transient measurements from an actual engine are affected by the heat

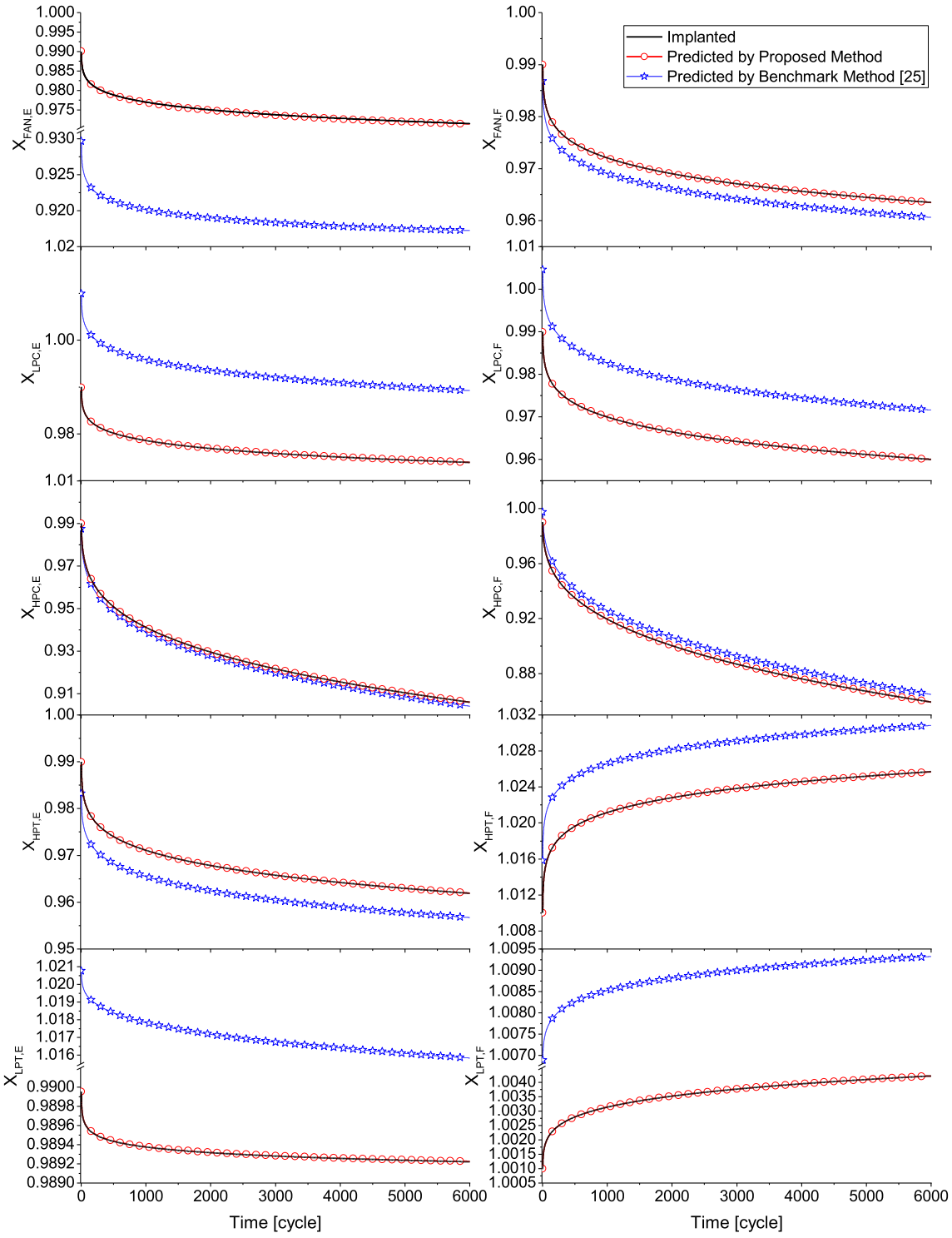

Fig. 11. Implanted and predicted damage propagation with and without consideration of heat soakage.

soakage and predicted engine health parameters would lead to inconsistent results, compensating for the delay in engine measurements. The delay caused by heat soakage will be considered as degradation in the diagnosis when heat soakage is ignored.

As mentioned before, the acceleration manoeuvre is selected for the fault diagnosis. The fuel schedule between 0.0 and 15.0 s (15.1 s in total) in Fig. 6, is selected in this study to conduct the fault diagnosis during the fault propagation. The initial point at the 0.0 s time instant in Fig. 6 is the beginning of the steady-state condition, and the remaining 15.0 s characterize the transient manoeuvre. The diagnostic process is based on Fig. 3, where the transient measurements will be used.

Fig. 11 demonstrates the fault propagation of implanted fault, predicted fault by proposed method and predicted fault by benchmark method [25]. It is clear that the predicted fault by the proposed method is very close to the implanted fault. In contrast, the degradation factors predicted by the benchmark method [25] are not as accurate as our proposed method. Further analysis of the average relative error of the health parameters reveals the accuracy of the developed diagnosis scheme under dynamic conditions shown in Fig. 12. It is evident that the highest prediction error for the transient diagnosis by the proposed and

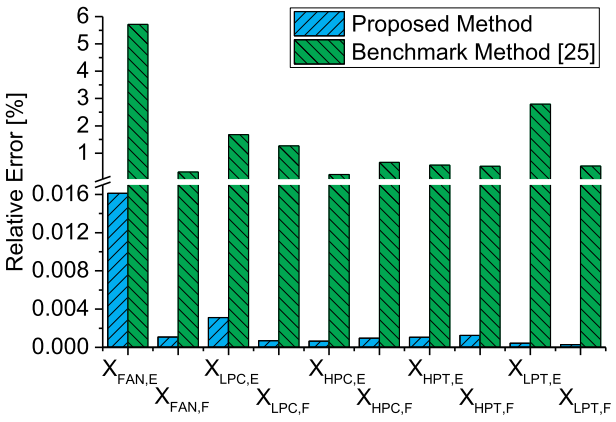

Fig. 12. Average prediction error of degradation factors in Case 2.

the benchmark methods are below 0.017% and 6% for all ten health parameters during the fault propagation, respectively.

Turning now to the computation efficiency on fault diagnosis, the average computation time and the number of operating points used along with the four sequential steps are shown in Table 8. For the proposed method, the average calculation time is 0.185, 1.624, 0.017, 0.013 s for four sequential steps, respectively. In Step 2, the prediction includes more variables, convergence criteria and sub-models than other steps, as shown in Fig. 3. Hence, the time consumption in Step 2 is significantly higher than the other steps. The mean computation time for fault diagnosis at each flight cycle is 1.839 s. Regarding the benchmark method [25], the average computation time for 6000 cycle during a 15.1 s transient manoeuvre is 30.688 s. In addition, the number of operation points for the four steps is also demonstrated in Table 8. Steps 1 and 2 use 151 operating points, where the first point is the steady-state operation point before the dynamic manoeuvre, and the remaining points are the measurements under the transient condition with heat soakage considered.

From the diagnostic accuracy and computational efficiency perspectives, the comparison of these results reveals that the proposed method is superior to the benchmark method [25] in both diagnostic accuracy and computational efficiency. Regarding the model complexity, the proposed method requires expert knowledge in the performance modelling of aero engines, for effective utilization of the diagnosis, whereas in the benchmark method [25] the user does not need to know the detailed modelling information inside the components. However, compared with existing model-based techniques [25], the significant improvement in accuracy and efficiency of this method offsets this limitation.

4.4. *Case 3: Impact of engine degradation on fuel consumption and payload*

The aircraft flight trajectory normally includes the following phases: takeoff, initial climb, climb, cruise, initial descent, descent, and landing. The majority of engine fuel is consumed during the takeoff, initial climb, climb, and cruise segments [53]. Hence, the fuel consumption during descent and landing is ignored in this study. Table 9 indicates a flight segment for estimating fuel consumption among flight trajectories during fault propagation. The duration of each flight phase is captured from Fig. 4 based on a flight trajectory of Shandong Airlines. The cruise thrust

Table 9
Typical Flight Segment.

Flight Segment	Altitude [m]	*MN*	Duration (min)	Net thrust [N]
Takeoff	0	0.2	1	89,411
Initial Climb	6100	0.57	16	43,200
Climb	10,600	0.66	6	27,294
Cruise	11,000	0.8	165	24,376

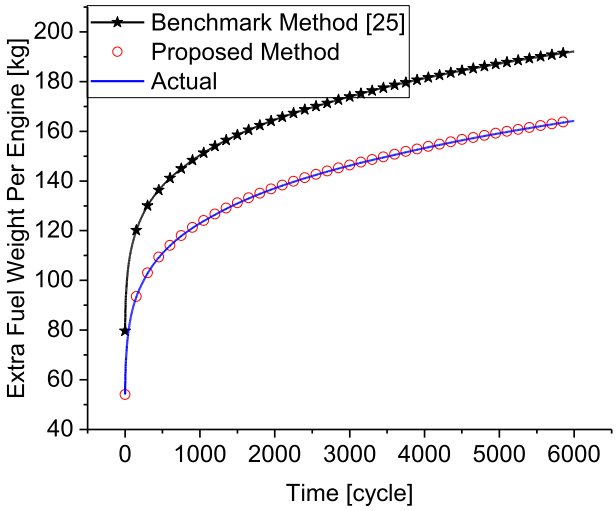

Fig. 13. Extra Fuel weight needed along fault propagation for each engine.

of the CFM56-7B engine is used as a reference value, and the other

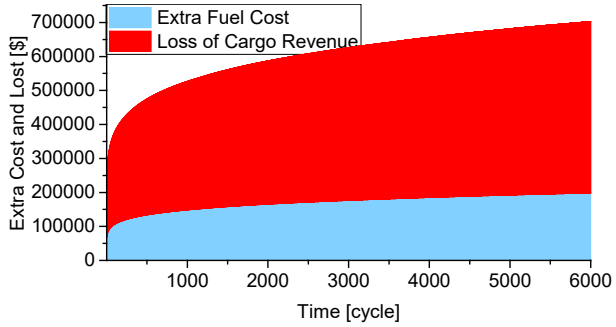

Fig. 14. Profit loss caused by extra fuel cost and loss of cargo revenue of aircraft fleet.

values of the thrust are estimated based on the ratio of each flight segment to the cruise thrust [54].

The actual and predicted degradation factors in Case 2 are injected into the engine model to maintain the same thrust and determine the corresponding fuel consumption. Fig. 13 shows a representation of the extra fuel weight required to maintain the same thrust in Table 9, along with the fault propagation for each engine by Eq. **(3)**. It is worth emphasizing that the extra fuel weight predicted by the proposed method will be considered as true value due to the low prediction error (Fig. 13).

Table 8
Computational efficiency of the diagnostic model in Case 2.

Parameter	Symbol	Unit	Proposed Method				Benchmark Method [25]
			Step 1	Step 2	Step 3	Step 4	
Run Time	*RT*	Second	0.185	1.624	0.017	0.013	30.688
Operating Point	*n*	–	151	151	1	1	151

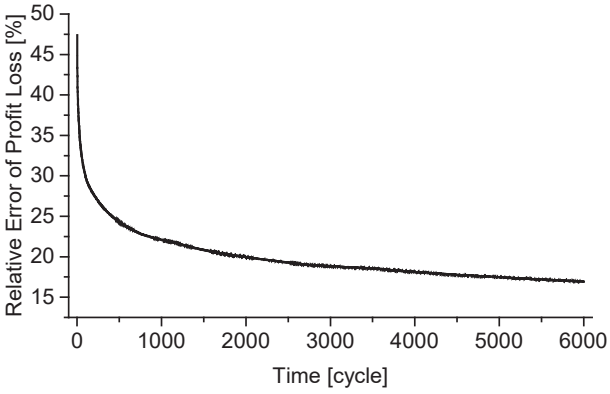

Fig. 15. Relative Error of Profit Loss by Benchmark Method in Comparison with Proposed Method.

If the same take-off weight of the aircraft is maintained, the payload weight needs to be decreased correspondingly to compensate for the extra fuel weight when the engine is degraded. After engine degradation, the extra fuel will not only increase the fuel cost during flight missions but also decrease the revenue of payload. The fuel cost of hydrogen and air freight rate of payload are 5.0 $/kg [55] and 12.66 $/kg [56], respectively.

Take the Shandong Airlines presented in Fig. 4 as an example, by Jan 1, 2021, the Shandong Airlines depicted in Fig. 4 has 121 Boeing 737–800 aircraft in the fleet [57] where aircraft is powered by two CFM56-7B turbofan engines. Fig. 14 presents the extra fuel cost and loss of cargo revenue along with the fault propagation for the entire fleet of 121 aircraft that can be calculated by Eqs. (4)-(5) based on the health parameters obtained by the proposed method. It is clear from Fig. 14 that the combined effect of multiple engine component degradation of the turbofan engines has a substantial impact on the economics of the airline fleet. The extra fuel cost starts at $65,423 and grows exponentially to $198,920 after 6000 cycles for the entire fleet. A similar pattern is shown for the loss of revenue due to loss of payload, which starts from $165,651 to $503,665 along with fault propagation. Fig. 15 demonstrates the relative error of the profit loss when compared to the proposed method. The relative error will be decreased during the fault propagation as the ratio of fuel weight prediction error over actual extra fuel weight is decreased (Fig. 13). However, the prediction error is still larger by 15% and the incorrect fuel weight prediction can increase the probability for flight associated risks.

Several attempts should be made to implement the proposed fault diagnosis method in real life applications from a practical perspective. Prior to analysing the characteristic performance data, the measurement noise filter and sensor validation should be checked for each sensor. There is no doubt that the performance model is critical for the model-based fault diagnosis. On completion of performance modelling, the process of components' map adaptation is highly recommended to be carried out. Once any engine maintenance action is completed, it is necessary to employ the map adaptation for the purpose of refining the baseline performance for the engine.

The findings of this study have a number of important implications for future practice in engine health management and mission analysis. Both of these trends could feed an optimization algorithm in order to improve the condition-based maintenance of the engines. Striking a balance between the cost of maintenance/downtime and restoring an engine's performance to economically efficient levels is a challenging process that can be further improved by utilising the proposed method.

Further investigation could focus on the schedule of condition-based maintenance and condition-based production to prolong the aero engine on-wing life, optimize flight mission profile, reduce maintenance cost, improve thermal efficiency, and promote aviation transport safety.

5. Conclusions

This paper describes the development of a sequential diagnostic method and its application to an aero engine with the primary aim of evaluating its accuracy and efficiency under steady-state and transient operating conditions. The results of this study demonstrate and illustrate that the sequential method could assess the fault state of multiple components that are degraded simultaneously when the bypass ratio changes with respect to the operating conditions. One of the advantages of this method is its ability to accurately diagnose all engine components' degradation level at transient conditions with high computational efficiency while considering heat soakage effects. Overall, this study amplifies the suitability of the sequential approach for effective and accurate turbofan engine fault diagnosis.

The conclusions drawn from this study are as follows:

- Firstly, this study focuses on determining the predictive validity of the developed engine performance model by comparing it with GasTurb and establishing a benchmark for fault diagnosis. The maximum relative error for the steady-state and transient conditions are less than 0.86% and 0.92%, respectively.
- For the fault diagnosis under steady-state conditions, the maximum average relative error for five rotating components that experience degradation simultaneously during a 6000-flight cycle period is less than 0.006%, and the mean computation time for the diagnosis is 0.081 s.
- Regarding fault diagnosis at dynamic conditions, the maximum mean relative error for five simultaneously degraded components is less than 0.016%, while the average computation time is only 1.839 s for a 15.1 s manoeuvre.
- The fault propagation will deteriorate the fuel consumption and cargo revenue. At 6000th flight cycle, the loss caused by gas path deterioration is 702,585 $ during a typical flight mission for an entire 121 aircraft fleet.

One of the proposed method's major advantages is that it can accurately diagnose the fault level of gas turbine engines under both steady-state and transient operating conditions in real-time. Another advantage of the developed method is that the heat soakage is considered in the transient model, which is more grounded in reality for those gas turbines with large thermal inertia. The desirable feature of the proposed method motivates the inclusion of the effect of component volume and the delay of fuel pump actuator during dynamic operating conditions; tasks that the authors are currently engaged in.

Overall, our study provides additional support for aero engine fault diagnosis and can potentially improve condition-based maintenance, which in turn will have a positive impact on the reliability, availability, efficiency, and cost reduction of gas turbines. In terms of future work, it would be interesting to explore the effects of fault propagation on hot section thermo-mechanical life for optimal condition-based production planning.

CRediT authorship contribution statement

Yu-Zhi Chen: Conceptualization, Investigation, Methodology, Software, Writing – original draft. **Elias Tsoutsanis:** Conceptualization, Methodology, Visualization, Writing – review & editing. **Heng-Chao Xiang:** Methodology, Writing – review & editing. **Yi-Guang Li:** Methodology, Writing – review & editing. **Jun-Jie Zhao:** Methodology, Writing – review & editing.

Declaration of Competing Interest

The authors declare that they have no known competing financial interests or personal relationships that could have appeared to influence the work reported in this paper.

Acknowledgments

This work is supported by the National Science and Technology Major Project under Grant No. 2017-V-0011-0062, and the Nature Science Foundation of Shaanxi under Grant No. NO. 2020JM-149.

Appendix A

A.1. Engine model

A thermodynamic model for an industrial triple-shaft engine has been developed and validated in our previous work [29]. In this study, five additional elements (i.e., fan, exhaust nozzle, shaft, first-order lag, and heat soakage) are developed and integrated into the performance model of a turbofan engine for both steady-state and transient conditions.

- Fan Model

The corrected engine shaft rotational speed (CN) could be obtained by Eq. (A.1) [58] when the inlet condition and rotational speed (N) are both known.

$$CN = \frac{(N/\sqrt{T_{in}})_{OD}}{(N/\sqrt{T_{in}})_{DP}} \tag{A.1}$$

The bypass pressure ratio (PR_{BP}) is guessed during performance modelling, and the fan performance map is employed to find the component performance as follows:

$$[CM_{in}, Eff_{BP}] = MAP(CN, PR_{BP}) \tag{A.2}$$

Hence, the bypass pressure at the fan outlet could be calculated as [59,60]:

$$P_{out} = P_{in} \bullet PR \tag{A.3}$$

Then, the core pressure ratio (PR_{Core}) is referred to Eq. (A.4) [61] as follows:

$$\left(\frac{PR_{Core}-1}{PR_{BP}-1}\right)_{OD} = \left(\frac{PR_{Core}-1}{PR_{BP}-1}\right)_{DP} \tag{A.4}$$

Compression efficiency of the fan at bypass flow (Eff_{BP}) could be determined by Eq. (A.2). Furthermore, the compression efficiency of the fan at core flow (Eff_{Core}) could be computed as follows [61]:

$$\left(\frac{Eff_{Core}}{Eff_{BP}}\right)_{OD} = \left(\frac{Eff_{Core}}{Eff_{BP}}\right)_{DP} \tag{A.5}$$

The corrected mass flow at the fan inlet (CM_{in}) could also be obtained by fan map by Eq. (A.2), and the mass flow rate at fan inlet is given by Eq. (A.6) [62].

$$W_{in} = CM_{in} \bullet \frac{P_{in}/P_{SLS}}{\sqrt{T_{in}/T_{SLS}}} \tag{A.6}$$

The mass flow rate of the core flow could be calculated by Eq. (A.7).

$$W_{Core} = W_{in}/(1+BPR) \tag{A.7}$$

The mass flow rate of the bypass flow could be obtained by Eq. (A.8).

$$W_{BP} = (W_{in} \bullet BPR)/(1+BPR) \tag{A.8}$$

As the efficiency, pressure ratio, and mass flow rate of the core flow and the bypass flow are determined, the outlet condition of the core flow and the bypass flow could be computed easily and similar to the compressor model [29].

- Exhaust Model

The computational process of the nozzle model includes six parts. The analysis of the sonic condition is conducted first to check the state of flow when the Mach number (MN) is close to 1. Then, the critical nozzle area will be calculated to determine whether the flow is under super-critical or sub-critical conditions. Consequently, the nozzle area (A_{loc}) required to expand the flow could be calculated for the specified condition. Once the flow state in the nozzle is obtained, the gross thrust will be computed. The relative error between A_{loc} and nozzle area at design point (A_{DP}, fixed nozzle area in this study) should be minimized with a pre-defined threshold after the iteration of engine performance simulation.

- Sonic condition

The sonic condition of the nozzle could be determined when the inlet condition is known. The detailed steps are explained as follows. Firstly, the temperature at sonic condition, t_{sn}, is guessed in order to obtain the gas property under sonic condition by Eq. (A.9), where MN equals to one. The γ_{sn} in Eq. (A.9) could be initially guessed based on total temperature and total pressure provisionally and be updated when the static temperature and static entropy are known.

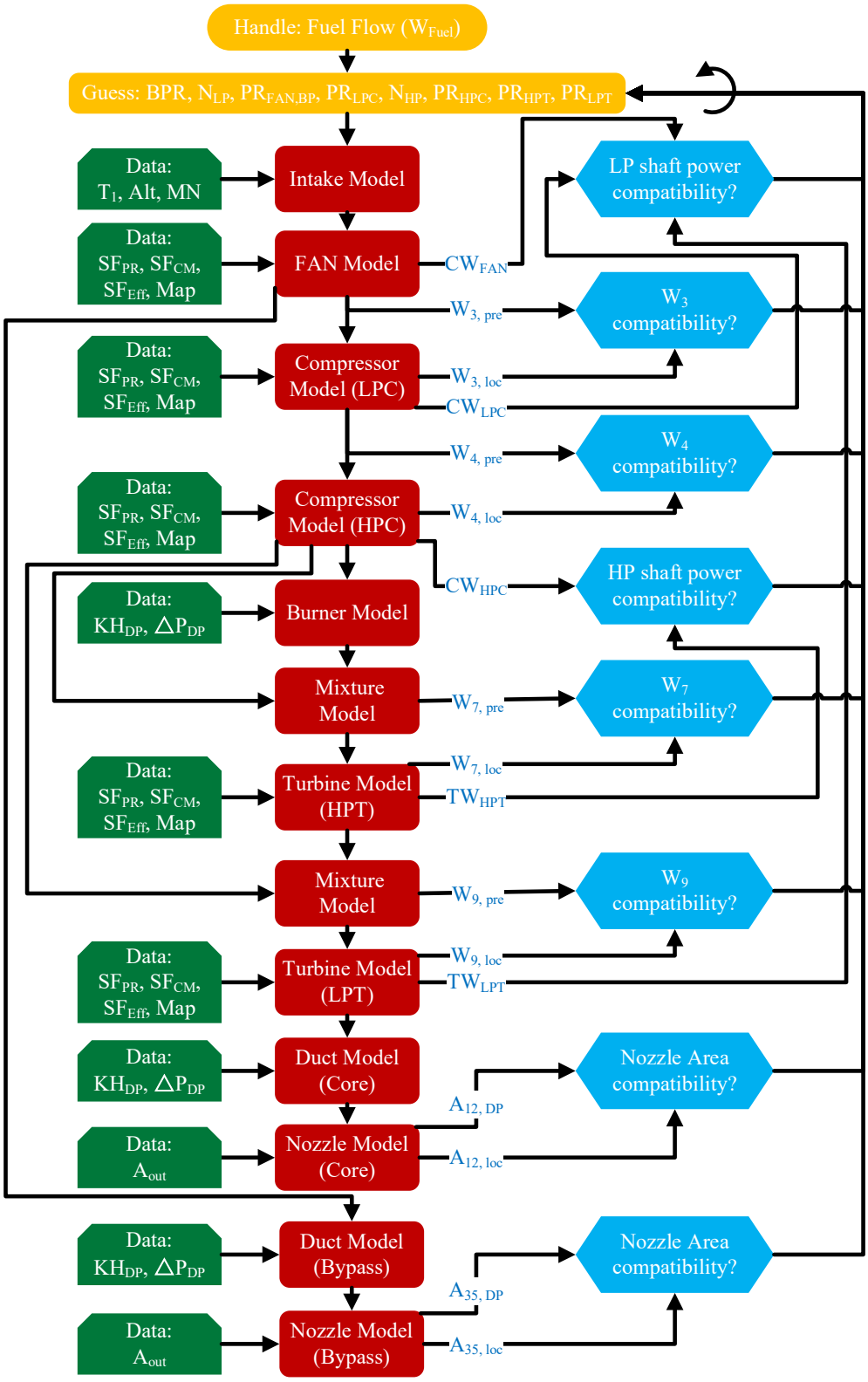

Fig. A1. Performance simulation process at steady-state conditions.

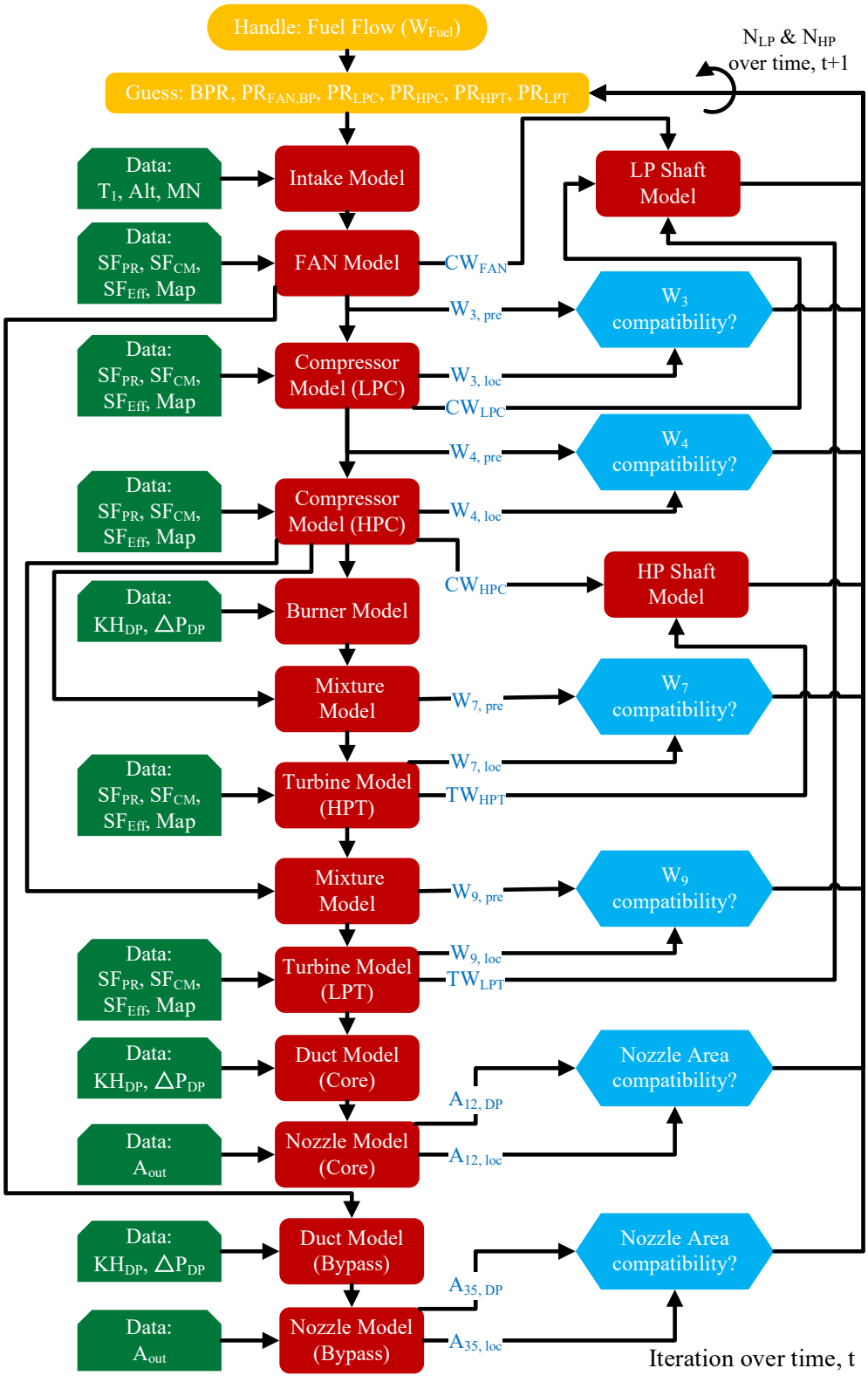

Fig. A2. Performance simulation process at dynamic conditions.

$$t_{sn} = \frac{T_{out}}{1 + MN^2 \bullet \frac{\gamma_{sn}-1}{2}} \tag{A.9}$$

Then, the static gas properties could be obtained by Eq. (A.10) assuming an isentropic process is employed.

$$[R_{sn}, \gamma_{sn}, h_{sn}, p_{sn}, \rho_{sn}] = GasProp_{[S,T]}(s_{sn}, t_{sn}, FAR, WAR) \tag{A.10}$$

The gas velocity at sonic condition (V_{sn}) could be obtained as follows:

$$V_{sn} = \sqrt{2(H_{in} - h_{sn})} \tag{A.11}$$

where H_{in} is inlet total enthalpy.

The *MN* under the specified static condition could be calculated as follows:

$$MN = V_{sn} / \sqrt{\gamma_{sn} \bullet R_{sn} \bullet t_{sn}} \tag{A.12}$$

The *MN* should be close to 1 within a pre-defined threshold, the iterations of the t_{sn} calculation will be terminated or the t_{sn} will be updated by Eq. (A.10) to find the sonic condition.

- Critical nozzle area

Then, the critical nozzle area (A_{crit}) could be determined by Eq. (A.13).

$$A_{crit} = W_{out} / (\rho_{sn} \bullet V_{sn}) \tag{A.13}$$

If $A_{out,DP}$ is less or equal to A_{crit}, the nozzle is working under super-critical condition and vice-versa.

- Sub-critical condition

Under sub-critical conditions, the outlet static pressure (p_{out}) is equal to the ambient pressure (p_{amb}). The remaining state parameters of the gas property could be computed by Eq. (A.14).

$$[V_{out}, \rho_{out}, t_{out}] = GasProp_{[S,P]}(s_{out}, p_{out}, FAR, WAR) \tag{A.14}$$

Hence, the required nozzle area could be obtained as follows:

$$A_{loc} = W_{in} / (\rho_{out} \bullet V_{out}) \tag{A.15}$$

- Super-critical condition

As the engine in concern is manufactured with a convergence nozzle, the maximum *MN* can only be equal to 1 for the super-critical condition. Hence, the nozzle outlet density (ρ_{out}), and velocity (V_{out}) is equal to ρ_{sn}, and V_{sn} in such a situation. The required nozzle area could be obtained by Eq. (A.15).

- Net thrust

Net thrust (*NG*) could be computed by Eq. (A.16).

$$NG = W_{in} \bullet (V_{out} - V_0) \bullet C_{FG} + 101325(p_{out} - p_{atm}) \bullet A_{out} \tag{A.16}$$

Where V_0 is the flight velocity and C_{FG} is nozzle coefficient from the component map.

- Iteration error

The residual error of the nozzle (E_{NZ}) during engine performance calculation iterations could be obtained by Eq. (A.17) [63].

$$E_{NZ} = \frac{A_{loc} - A_{DP}}{A_{DP}} \tag{A.17}$$

- Shaft Model

The shaft torque balance among turbine work (*TW*), compressor work (*CW*) and auxiliary work (*AW*) is not satisfied during dynamic operations such as acceleration and deceleration. The surplus power (*SP*) of each shaft could be obtained based on the imbalance in torque calculated by Eq. (A.18) [64].

$$SP = TW - CW - AW = \frac{4\pi^2}{3600} \bullet I \bullet N \bullet \frac{dN}{dt} \tag{A.18}$$

where *I* is shaft inertia.

The shaft speed for the next step is updated by the increment of rotation speed and shaft speed at the previous time step as follows:

$$N(t+\Delta t) = N(t) + \frac{dN}{dt} \bullet \Delta t \tag{A.19}$$

where Δt is the time step.

- First-order Lag

The first-order lag is applied to represent the time delay phenomenon of the engine rotor under dynamic manoeuvring [65,66] as follows:

$$\frac{N_{out}(s)}{N_{in}(s)} = \frac{1}{\tau \bullet s + 1} \tag{A.20}$$

where τ is the time constant for the system, $N_{out}(s)$ is the value of the input with defined input delay and $N_{in}(s)$ is the input value without delay.

- Heat Soakage Model

The heat transfer between gas flow and engine metal is obtained by Eq. **(A.21)** with exponential decay [43].

$$Q = U_{ht} \bullet A_{ht}(T_g - T_m) \bullet (e^{-\Delta t/\tau} - 1) \tag{A.21}$$

where Q is heat energy, U_{ht} is heat transfer coefficient, A_{ht} is effective contact surface, T_g is gas temperature, T_m is metal temperature, Δt is time step, and τ is time constant.

The heat transfer coefficient is determined by Eq. **(A.22)** [67].

$$U_{ht} = \frac{1}{\frac{1}{FC} + \frac{l_{eff}}{k_m}} \tag{A.22}$$

The time constant is calculated by Eq. (A.23) [67].

$$\tau = \frac{c_m \bullet W_m}{U_{ht} \bullet A_{ht}} \tag{A.23}$$

where W_m is effective mass, c_m is the specific heat of the component's material.

The average material temperature (T_m) could be computed as follows [67]:

$$\frac{dT_m}{dt} = \frac{Q}{c_m \bullet W_m} \tag{A.24}$$

The enthalpy drop of gas (ΔH_g) could be determined by Eq. **(A.25)**. Then, the gas temperature after heat transfer could be calculated as the gas pressure and enthalpy are known.

$$\Delta H_g = \frac{Q}{W_g} \tag{A.25}$$

where W_g is mass flow rate of gas.

A.2. Calculating process of aero engine thermodynamic model for CFM56-7B

The aero engine thermodynamic model is based on the models described in the methodology part and our previous work [29], which is applicable for different types of gas turbine engines. The calculating process of steady-state performance simulation is shown in Fig. A1, where eight iteration variables are needed, which are BPR, N_{LP}, $PR_{FAN,BP}$, PR_{LPC}, N_{HP}, PR_{HPC}, PR_{HPT}, PR_{LPT}. Correspondingly, eight balance equations that should be satisfied are listed in Fig. A1 by blue blocks. Likewise, the calculating process of dynamic performance of the turbofan in concern is demonstrated in Fig. A2, where six independent variables, i.e. BPR, $PR_{FAN,BP}$, PR_{LPC}, PR_{HPC}, PR_{HPT}, $PR_{LPT}$are invloved. Six equations associated with the independent variables are illustrated in Fig. A2 by blue blocks. The two shaft rotational speeds are updated by the shaft model described in Appendix A.1. It is worth emphasizing that the heat soak is integrated into the component models.

References

[1] Aydin G. The modeling and projection of primary energy consumption by the sources. Energy Sources Part B 2015;10:67–74.

[2] Feng YY, Zhang LX. Scenario analysis of urban energy saving and carbon abatement policies: A case study of Beijing city, China. Procedia Environ Sci 2012; 13:632–44.

[3] Aydin G. The application of trend analysis for coal demand modeling. Energy Sources Part B 2015;10:183–91.

[4] Weimann L, Gabrielli P, Boldrini A, Kramer GJ, Gazzani M. Optimal hydrogen production in a wind-dominated zero-emission energy system. Adv Appl Energy 2021;3:100032.

[5] Schorn F, Breuer JL, Samsun RC, Schnorbus T, Heuser B, Peters R, et al. Methanol as a renewable energy carrier: An assessment of production and transportation costs for selected global locations. Adv Appl Energy 2021;3:100050.

[6] Martínez-Gordón R, Sánchez-Diéguez M, Fattahi A, Morales-España G, Sijm J, Faaij A. Modelling a highly decarbonised North Sea energy system in 2050: A multinational approach. Adv Appl Energy 2022;5:100080.

[7] Aydin G, Karakurt I, Aydiner K. Analysis and Mitigation Opportunities of Methane Emissions from the Energy Sector. Energy Sources Part A 2012;34:967–82.

[8] Consonni S, Mastropasqua L, Spinelli M, Barckholtz TA, Campanari S. Low-carbon hydrogen via integration of steam methane reforming with molten carbonate fuel cells at low fuel utilization. Adv Appl Energy 2021;2:100010.

[9] Wang Y, Yuan H, Martinez A, Hong P, Xu H, Bockmiller FR. Polymer electrolyte membrane fuel cell and hydrogen station networks for automobiles: Status, technology, and perspectives. Adv Appl Energy 2021;2:100011.

[10] International Civil Aviation Organization (ICAO). Forecasts of Scheduled Passenger and Freight Traffic. ICAO / Economic Development of Air Transport 2018. https://www.icao.int/sustainability/Pages/eap-fp-forecast-scheduled-passenger-traffic.aspx (accessed March 16, 2021).
[11] Magrini A, Benini E, Yao HD, Postma J, Sheaf C. A review of installation effects of ultra-high bypass ratio engines. Prog Aerosp Sci 2020;119:100680.
[12] Zaidan MA, Relan R, Mills AR, Harrison RF. Prognostics of gas turbine engine: An integrated approach. Expert Syst Appl 2015;42:8472–83.
[13] Hanachi H, Liu J, Kim IY, Mechefske CK. Hybrid sequential fault estimation for multi-mode diagnosis of gas turbine engines. Mech Syst Sig Process 2019;115:255–68.
[14] Talebi SS, Tousi AM. The effects of compressor blade roughness on the steady state performance of micro-turbines. Appl Therm Eng 2017;115:517–27.
[15] Simon DL, Rinehart AW. Sensor Selection for Aircraft Engine Performance Estimation and Gas Path Fault Diagnostics. J Eng Gas Turbines Power 2016;138:1–11.
[16] Tahan M, Tsoutsanis E, Muhammad M, Abdul Karim ZA. Performance-based health monitoring, diagnostics and prognostics for condition-based maintenance of gas turbines: A review. Appl Energy 2017;198:122–44.
[17] Sampath S, Ogaji SOT, Li YG, Singh R. Fault diagnosis of a two spool turbo-fan engine using transient data: A genetic algorithm approach. American Society of Mechanical Engineers, International Gas Turbine Institute, Turbo Expo (Publication). IGTI 2003;1:351–9.
[18] Safiyullah F, Sulaiman SA, Naz MY, Jasmani MS, Ghazali SMA. Prediction on performance degradation and maintenance of centrifugal gas compressors using genetic programming. Energy 2018;158:485–94.
[19] Tsoutsanis E, Hamadache M, Dixon R. Real-Time Diagnostic Method of Gas Turbines Operating Under Transient Conditions in Hybrid Power Plants. J Eng Gas Turbines Power 2020;142:1–10.
[20] Lu F, Gao T, Huang J, Qiu X. A novel distributed extended Kalman filter for aircraft engine gas-path health estimation with sensor fusion uncertainty. Aerosp Sci Technol 2019;84:90–106.
[21] Tang S, Tang H, Chen M. Transfer-learning based gas path analysis method for gas turbines. Appl Therm Eng 2019;155:1–13.
[22] Zhou D, Yao Q, Wu H, Ma S, Zhang H. Fault diagnosis of gas turbine based on partly interpretable convolutional neural networks. Energy 2020;200:117467.
[23] Lu J, Huang J, Lu F. Kernel extreme learning machine with iterative picking scheme for failure diagnosis of a turbofan engine. Aerosp Sci Technol 2020;96:105539.
[24] Bai M, Liu J, Chai J, Zhao X, Yu D. Anomaly detection of gas turbines based on normal pattern extraction. Appl Therm Eng 2020;166:114664.
[25] Li J, Ying Y. Gas turbine gas path diagnosis under transient operating conditions: A steady state performance model based local optimization approach. Appl Therm Eng 2020;170.
[26] Jaw LC, Mattingly JD. Aircraft engine controls: design, system analysis, and health monitoring. Reston, Va, USA: American Institute of Aeronautics and Astronautics, Inc; 2009.
[27] Hanachi H, Mechefske C, Liu J, Banerjee A, Chen Y. Performance-Based Gas Turbine Health Monitoring, Diagnostics, and Prognostics: A Survey. IEEE Trans Reliab 2018;67:1340–63.
[28] Fentaye AD, Baheta AT, Gilani SI, Kyprianidis KG. A review on gas turbine gas-path diagnostics: State-of-the-art methods, challenges and opportunities. Aerospace 2019;6.
[29] Chen Y, Zhao X, Xiang H, Tsoutsanis E. A sequential model-based approach for gas turbine performance diagnostics. Energy 2021;220:119657.
[30] Jasmani MS, Li YG, Ariffin Z. Measurement selections for multi-component gas path diagnostics using analytical approach and measurement subset concept. J Eng Gas Turbines Power 2011;133:1–10.
[31] Chen M, Quan HL, Tang H. An Approach for Optimal Measurements Selection on Gas Turbine Engine Fault Diagnosis. J Eng Gas Turbines Power 2015;137:071203.
[32] Xu J, Wang Y, Xu L. PHM-Oriented Sensor Optimization Selection Based on Multiobjective Model for Aircraft Engines. IEEE Sens J 2015;15:4836–44.
[33] Hu RL, Granderson J, Auslander DM, Agogino A. Design of machine learning models with domain experts for automated sensor selection for energy fault detection. Appl Energy 2019;235:117–28.
[34] Yu H, Zhensheng S, Lijia C, Yin Z, Pengfei P. Optimization configuration of gas path sensors using a hybrid method based on tabu search artificial bee colony and improved genetic algorithm in turbofan engine. Aerosp Sci Technol 2021;112.
[35] Ogaji S, Sampath S, Singh R, Probert D. Novel approach for improving power-plant availability using advanced engine diagnostics. Appl Energy 2002;72:389–407.
[36] Stamatis AG. Evaluation of gas path analysis methods for gas turbine diagnosis. J Mech Sci Technol 2011;25:469–77.
[37] Li J, Ying Y. A Method to Improve the Robustness of Gas Turbine Gas-Path Fault Diagnosis Against Sensor Faults. IEEE Trans Reliab 2018;67:3–12.
[38] Ogaji SOT, Sampath S, Li YG, Singh R. Gas Path Fault Dlagnosis of a Turbofan Engine from Transient Data Using Artificial Neural Networks. American Society of Mechanical Engineers. Int Gas Turbine Institute, Turbo Expo (Publication) IGTI 2003;1:405–14.
[39] Li YG. A gas turbine diagnostic approach with transient measurements. Proc Institution Mech Engineers, Part A: J Power Energy 2003;217:169–78.
[40] Tsoutsanis E, Meskin N, Benammar M, Khorasani K. Transient gas turbine performance diagnostics through nonlinear adaptation of compressor and turbine maps. J Eng Gas Turbines Power 2015;137:1–12.
[41] Tsoutsanis E, Meskin N, Benammar M, Khorasani K. A dynamic prognosis scheme for flexible operation of gas turbines. Appl Energy 2016;164:686–701.
[42] Tsoutsanis E, Meskin N. Derivative-driven window-based regression method for gas turbine performance prognostics. Energy 2017;128:302–11.
[43] Li Z-J, Li Y-G, Korakianitis T. Gas turbine transient performance simulation with simplified heat soakage model. ASME Turbo Expo: Turbomachinery Technical Conf Exposition 2020. p. GT2020-14484.
[44] Li YG. Gas turbine performance and health status estimation using adaptive gas path analysis. J Eng Gas Turbines Power 2010;132:1–9.
[45] Verbist M. Gas path analysis for enhanced aero-engine condition monitoring and maintenance. Delft University of Technology; 2017. PhD thesis.
[46] Plis M, Rusinowski H. A mathematical model of an existing gas-steam combined heat and power plant for thermal diagnostic systems. Energy 2018;156:606–19.
[47] Chen Y-Z, Li Y-G, Tsoutsanis E, Newby M, Zhao X-D. Techno-economic evaluation and optimization of CCGT power Plant: A multi-criteria decision support system. Energy Convers Manage 2021;237:114107.
[48] Chatterjee S, Litt JS. Online model parameter estimation of jet engine degradation for autonomous propulsion control. In: AIAA Guidance, Navigation, and Control Conference and Exhibit, Austin, Texas, USA: 2003, p. 1–17.
[49] Saxena A, Goebel K, Simon D, Eklund N. Damage propagation modeling for aircraft engine run-to-failure simulation. In: 2008 International Conference on Prognostics and Health Management, PHM 2008 2008.
[50] Flightadsb. Replay of flight SC8811 executed by a Boeing 737-800 powered by two CFM56-7B engines 2021. https://flightadsb.variflight.com/playbacksup/B7668/d3c2b69ea2714a65be6e4ea7fdb7e508/1623695748/1623712140 (accessed July 1, 2021).
[51] Kurzke J. GasTurb: A Program to Calculate Design and Off-Design Performance of Gas Turbines 2017.
[52] Cranfield University. Cranfield supports ZeroAvia's world first hydrogen-electric passenger aircraft flight 2020. https://www.cranfield.ac.uk/press/news-2020/cranfield-supports-zeroavias-world-first-hydrogen-electric-passenger-aircraft-flight (accessed May 13, 2021).
[53] Lissys Limited. Piano-X: Aircraft Emissions and Performance 2008.
[54] Kim S, Son C, Kim K. Combining effect of optimized axial compressor variable guide vanes and bleed air on the thermodynamic performance of aircraft engine system. Energy 2017;119:199–210.
[55] Papadias D, Ahluwalia RK, Connelly E, Devlin P. Total Cost of Ownership (TCO) Analysis for Hydrogen Fuel Cells in Maritime Applications. Argonne National Lab 2020.
[56] Chao CC, Li RG. Effects of cargo types and load efficiency on airline cargo revenues. Journal of Air Transport Management 2017;61:26–33.
[57] Shandong Airlines. Shandong Airlines Profile 2021. https://www.sda.cn/about/memorabilia/ (accessed August 1, 2021).
[58] Wang L, Lin X, Zhang H, Peng L, Chen H. Brayton-cycle-based pumped heat electricity storage with innovative operation mode of thermal energy storage array. Appl Energy 2021;291:116821.
[59] Kim MJ, Kim TS, Flores RJ, Brouwer J. Neural-network-based optimization for economic dispatch of combined heat and power systems. Appl Energy 2020;265:114785.
[60] Zhang H, Wang L, Lin X, Chen H. Combined cooling, heating, and power generation performance of pumped thermal electricity storage system based on Brayton cycle. Appl Energy 2020;278:115607.
[61] Kurzke J, Halliwell I. Propulsion and Power: An Exploration of Gas Turbine Performance Modeling. Cham, Switzerland: Springer International Publishing AG, part; 2018.
[62] Zheng J, Chang J, Ma J, Yu D. Modeling and analysis of windmilling operation during mode transition of a turbine-based-combined cycle engine. Aerosp Sci Technol 2021;109:106423.
[63] Zhang J, Tang H, Chen M. Linear substitute model-based uncertainty analysis of complicated non-linear energy system performance (case study of an adaptive cycle engine). Appl Energy 2019;249:87–108.
[64] Kim S. A new performance adaptation method for aero gas turbine engines based on large amounts of measured data. Energy 2021;221.
[65] Tsoutsanis E, Meskin N. Dynamic performance simulation and control of gas turbines used for hybrid gas/wind energy applications. Appl Therm Eng 2019;147:122–42.
[66] Wei Z, Jafari S, Zhang S, Nikolaidis T. Hybrid Wiener model: An on-board approach using post-flight data for gas turbine aero-engines modelling. Appl Therm Eng 2021;184:116350.
[67] De Giorgi MG, Quarta M. Hybrid MultiGene Genetic Programming - Artificial neural networks approach for dynamic performance prediction of an aeroengine. Aerosp Sci Technol 2020;103.